

## THE INFRARED SPECTRA OF POLYCYCLIC AROMATIC HYDROCARBONS WITH EXCESS PERIPHERAL H ATOMS ( $H_n$ -PAHs) AND THEIR RELATION TO THE 3.4 AND 6.9 $\mu\text{m}$ PAH EMISSION FEATURES

SCOTT A. SANDFORD<sup>1</sup>, MAX P. BERNSTEIN<sup>1,2</sup>, AND CHRISTOPHER K. MATERESE<sup>3</sup>

<sup>1</sup> NASA-Ames Research Center, Mail Stop 245-6, Moffett Field, CA 94035-1000, USA; [Scott.A.Sandford@nasa.gov](mailto:Scott.A.Sandford@nasa.gov)

<sup>2</sup> NASA Headquarters, Mail Code 3K39, 300 East Street SW, Washington, DC 20546, USA

<sup>3</sup> SETI Institute, 189 Bernardo Avenue, Suite 100, Mountain View, CA 94043, USA

Received 2012 October 31; accepted 2013 January 11; published 2013 March 1

### ABSTRACT

Polycyclic aromatic hydrocarbons (PAHs) are likely responsible for the family of infrared emission features seen in a wide variety of astrophysical environments. A potentially important subclass of these materials are PAHs whose edges contain excess H atoms ( $H_n$ -PAHs). This type of compound may be present in space, but it has been difficult to assess this possibility because of a lack of suitable laboratory spectra to assist with analysis of astronomical data. We present 4000–500  $\text{cm}^{-1}$  (2.5–20  $\mu\text{m}$ ) infrared spectra of 23  $H_n$ -PAHs and related molecules isolated in argon matrices under conditions suitable for interpretation of astronomical data. Spectra of molecules with mixed aromatic and aliphatic domains show characteristics that distinguish them from fully aromatic PAH equivalents. Two major changes occur as PAHs become more hydrogenated: (1) aromatic C–H stretching bands near 3.3  $\mu\text{m}$  weaken and are replaced with stronger aliphatic bands near 3.4  $\mu\text{m}$ , and (2) aromatic C–H out-of-plane bending mode bands in the 11–15  $\mu\text{m}$  region shift and weaken concurrent with growth of a strong aliphatic  $-\text{CH}_2-$  deformation mode near 6.9  $\mu\text{m}$ . Implications for interpreting astronomical spectra are discussed with emphasis on the 3.4 and 6.9  $\mu\text{m}$  features. Laboratory data is compared with emission spectra from IRAS 21282+5050, an object with normal PAH emission features, and IRAS 22272+5435 and IRAS 0496+3429, two protoplanetary nebulae with abnormally large 3.4  $\mu\text{m}$  features. We show that “normal” PAH emission objects contain relatively few  $H_n$ -PAHs in their emitter populations, but less evolved protoplanetary nebulae may contain significant abundances of these molecules.

*Key words:* infrared: ISM – ISM: abundances – ISM: lines and bands – ISM: molecules – methods: laboratory – molecular data – techniques: spectroscopic

*Online-only material:* color figure

### 1. INTRODUCTION

It is now generally understood that polycyclic aromatic hydrocarbons (PAHs) and related materials are responsible for a family of infrared emission features, the largest of which fall near 3040, 1615, 1310, 1150, 885, and 785  $\text{cm}^{-1}$  (3.29, 6.2, 7.7, 8.7, 11.3, and 12.7  $\mu\text{m}$ ), that are seen in a wide variety of astrophysical environments (Allamandola et al. 1989a, 1989b, 1999; Peeters et al. 2002; Tielens 2008). The state of the populations of these compounds varies with environmental conditions and history, and at any given location the population may contain a mixture of normal PAHs in both neutral and ionized states, as well as molecular variants, including PAHs with attached chemical side groups, aromatic structures with five membered rings, skeletal structures containing heteroatoms, and deficits or excesses of peripheral H atoms (Allamandola et al. 1989a, 1989b, 1999).

Classical PAHs consist of various combinations of planar fused hexagonal carbon rings with hydrogen atoms terminating carbon bonds around the periphery of the molecule. In such molecules, all the carbon atoms participate in multiple aromatic ( $sp^2$ ) bonds. Such bonds are largely immune to disruption by UV photons and they give PAHs the stability they need to survive in the high radiation environments in which they are seen in space in emission (Allamandola et al. 1989b).

$H_n$ -PAHs are similar in overall structure to PAHs, except that they contain excess H atoms. The presence of these extra H atoms converts the flat aromatic ( $sp^2$ ) bonding of their associated C atoms into tetrahedral aliphatic ( $sp^3$ ) bonding. The resulting molecules are still cyclic, but contain both aromatic and aliphatic domains. The aliphatic domains cause the molecule to depart from planarity, and this can result in molecular stresses as

adjacent aromatic and aliphatic domains compete to preserve their preferred planar/tetrahedral configurations. This results in considerable breaking of molecular symmetries and increases the number of modes that are infrared active. Because of this, and because of the wider range of bonds present, these molecules produce infrared spectra that are often considerably more complex than those of either fully aliphatic molecules or normal, fully aromatic PAHs. In general,  $H_n$ -PAHs show a mixture of both aromatic and aliphatic spectral characteristics that are themselves modified by the mutual interactions of these two bonding structures (Bernstein et al. 1996).

The aliphatic bonds in  $H_n$ -PAHs are not as stable against photolytic disruption as are aromatic bonds of normal PAHs. As a result,  $H_n$ -PAHs would not be expected to be numerous in some of the more hostile astrophysical environments in which infrared emission by PAHs is seen. However, there is good reason to believe that  $H_n$ -PAHs should be present, perhaps even abundant, in more benign environments. For example, the unique spectral characteristics of  $H_n$ -PAHs may help explain some of the more atypical infrared emission spectra seen toward protoplanetary nebulae in which C-rich material is flowing outward from a central star that is not currently emitting large amounts of UV radiation (Bernstein et al. 1996).

Furthermore, PAHs in cold, dense interstellar molecular clouds are expected to be largely frozen into  $\text{H}_2\text{O}$ -rich, mixed molecular ices. Laboratory simulations have demonstrated that radiation processing of normal PAHs in such ices results in the conversion of some of the original PAHs into  $H_n$ -PAHs (Sandford et al. 2000; Bernstein et al. 1999, 2002). Thus,  $H_n$ -PAHs likely constitute a portion of the population of aromatic molecules in and around dense molecular clouds. In this

regard, it is interesting to note that the same radiation chemistry that produces  $H_n$ -PAHs is expected to result in enrichments of deuterium in the products (Sandford et al. 2000, 2001; Sandford 2002). Deuterium enrichments are seen in the carbonaceous fractions of primitive meteorites, interplanetary dust particles (IDPs), and cometary grains (e.g., McKeegan et al. 1985, 2006; Epstein et al. 1987; Cronin et al. 1993; Messenger 2000), and at least a portion of the carrier(s) of these deuterium enrichments appear to be associated with PAHs and other aromatic materials (Kerridge et al. 1987; Clemett et al. 1993; Aléon et al. 2000). Such enrichments are taken as evidence for the survival of the products of interstellar dense cloud chemistry (Zinner 1988).

Although ultraviolet, visible, and infrared spectra have been published of a handful of  $H_n$ -PAHs in Ar and  $H_2O$  matrices (Bernstein et al. 1996, 2005; Halasinski et al. 2005) and in the gas phase (Wagner et al. 2000), it has been difficult to assess the importance of  $H_n$ -PAHs in space because there has been a paucity of relevant laboratory infrared spectra of these species. In this paper, we present the 4000–500  $cm^{-1}$  (2.5–20  $\mu m$ ) infrared spectra of 23  $H_n$ -PAHs and related molecules that range in size from 2 to 7 rings and in excess H coverage from one extra H atom to fully hydrogenated species (cyclic aliphatics). Spectra were taken from molecules isolated in argon at 15 K. Molecules measured in this manner provide spectra that are well suited to the interpretation of spectra produced by interstellar PAHs (Allamandola et al. 1999) and this technique has been successfully used in the past on a variety of PAHs and related aromatic species, including, for example, neutrals (Hudgins & Sandford 1998a, 1998b, 1998c), ions (Hudgins et al. 1994; Hudgins & Allamandola 1995a, 1995b, 1997), deuterated PAHs (Bauschlicher et al. 1997; Peeters et al. 2004), PAHs with side groups (Langhoff et al. 1998), and PAHs that contain skeletal heteroatoms like nitrogen (Mattioda et al. 2003). In the following sections, we describe the experimental techniques and equipment used to obtain the spectra of the  $H_n$ -PAHs we have examined, present the data, discuss how the spectra of these molecules differ from normal PAHs, and describe some of the spectral patterns associated with these molecules. Finally, we discuss how these molecules might best be detected in space and what implications their presence may have for the interpretation of astronomical data, particularly for the interpretation of data from protoplanetary nebulae and areas in which star formation is releasing the materials held in ices in dense clouds.

## 2. EXPERIMENTAL TECHNIQUES

Standard inert matrix isolation techniques were used to isolate individual  $H_n$ -PAH molecules in an argon matrix in which their infrared spectra were measured. The experimental apparatus and methodology have been described in detail previously (Hudgins et al. 1994; Hudgins & Allamandola 1995a, 1995b; Bauschlicher et al. 1997; Hudgins & Sandford 1998a, 1998b, 1998c) and are reviewed only briefly here.

An infrared transparent sample window (CsI) was suspended inside a high-vacuum chamber ( $P \sim 10^{-8}$  torr) and cooled by a closed-cycle Helium refrigerator. The vacuum chamber is arranged in such a way that the cooled sample window can be freely rotated to face multiple gas inlet ports and optical ports without the need to break vacuum. Spectra were measured by inserting the sample chamber, which was equipped with CsI vacuum windows, into the sample compartment of a Nicolet FTIR spectrometer. Initially, the CsI sample window was cooled to 15 K and an infrared spectrum was obtained of the blank cold window. Mid-infrared spectra (4000–500  $cm^{-1}$ ) were collected

using an MCT-B detector/KBr beamsplitter combination. All spectra reported here were measured at a resolution of 0.9  $cm^{-1}$  (the width of an unresolved line) using a data-sampling spacing of 0.23  $cm^{-1}$ .

Once an infrared spectrum had been obtained from the blank sample window, the window was rotated to face two sample deposition inlets. Samples were prepared by co-deposition of a gaseous  $H_n$ -PAH with a large overabundance of argon until a sample with appropriate thickness was produced.

The  $H_n$ -PAHs were deposited from resistively heated pyrex tubes mounted on one of the sample chamber inlets. Sample temperatures during vaporization were monitored using a type K thermocouple mounted on the exterior of the tube. During  $H_n$ -PAH volatilization, a large overabundance of argon was admitted through an adjacent inlet port in such a way that the two “streams” coalesced and froze together on the surface of the cold window. The argon deposition line was passed through a liquid nitrogen trap to minimize contamination from  $H_2O$  and other condensibles, and the Ar flow rate was adjusted to ensure deposited  $H_n$ -PAHs were well-isolated in the resulting solid matrix. Optimal argon flow rates were generally between 0.5 and 1.0  $mmol\ hr^{-1}$ . On the basis of this flow rate and the  $H_n$ -PAH deposition rates calculated from integrated band areas and using available theoretical intrinsic band strengths (or typical values for relevant functional groups in cases where theoretical values are not available), the argon/ $H_n$ -PAH ratios in all samples are estimated to have been well in excess of 1000/1, ensuring that trapped  $H_n$ -PAHs were well-isolated. Typical samples had total thicknesses of  $\sim 0.1\ \mu m$ .

The  $H_n$ -PAHs used in this investigation are summarized in Table 1. The table provides, for each  $H_n$ -PAH: (1) a series identifier letter (related  $H_n$ -PAH structures are placed in the same series); (2) the full molecular name and source—either Aldrich, The Thermodynamics Research Center at Texas A&M synthesized by Ronald G. Harvey (TRC), or the laboratory of John C. Fetzer (JCF); (3) an abbreviated name or acronym; (4) a molecular formula; and (5) a structure.  $H_n$ -PAH samples were used without further purification. Matheson prepurified argon (99.998% min.) was used as the matrix material.

After sample deposition was complete, the cold head was rotated back to face the beam of the infrared spectrometer and spectra were taken of the sample window and the Ar: $H_n$ -PAH sample layer frozen on its surface. This spectrum was then ratioed to that of the blank cold window to produce a final transmission spectrum of the Ar: $H_n$ -PAH sample. Band strengths were integrated from absorbance spectra using an algorithm provided with the spectrometer. We provide spectra and tabulated band strengths for the  $H_n$ -naphthalenes (Series A) in the main body of this paper; the Appendix contains similar materials for all the other series listed in Table 1.

## 3. EXPERIMENTAL RESULTS

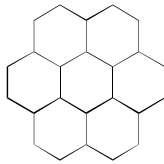
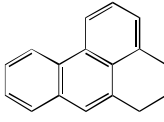
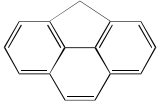
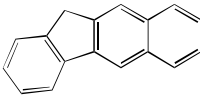
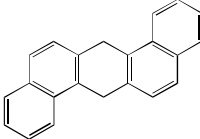
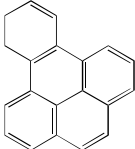
### 3.1. Basic Spectroscopy of PAH and $H_n$ -PAH Molecules

The spectra of purely aromatic PAHs all contain a prominent system of features in the 3150–2970  $cm^{-1}$  (3.18–3.37  $\mu m$ ) region (see, for example, Hudgins & Sandford 1998a, 1998b, 1998c). The strongest of these bands are due to C–H stretching modes of peripheral H atoms bonded to aromatic ( $sp^2$ ) C atoms, although some of these features can be associated with overtone/combination modes. The strongest of the C–H stretching fundamentals typically falls in the 3080–3040  $cm^{-1}$  (3.25–3.29  $\mu m$ ) range.

**Table 1**  
The H<sub>n</sub>-PAHs Examined in this Study

Series	H <sub>n</sub> -PAH Name	Abbreviation	Formula	Structure
A	1,2-dihydronaphthalene (Aldrich)	DHN	C <sub>10</sub> H <sub>10</sub>	
A	1,2,3,4-tetrahydronaphthalene (Aldrich)	THN	C <sub>10</sub> H <sub>12</sub>	
A	1,2,3,4,5,6,7,8-octahydronaphthalene (Aldrich)	OHN	C <sub>10</sub> H <sub>16</sub>	
A	<i>cis</i> -decahydronaphthalene (Aldrich)	<i>c</i> -PHN	C <sub>10</sub> H <sub>18</sub>	
A	<i>trans</i> -decahydronaphthalene (Aldrich)	<i>t</i> -PHN	C <sub>10</sub> H <sub>18</sub>	
B	9,10-dihydroanthracene (Aldrich)	DHA	C <sub>14</sub> H <sub>12</sub>	
B	1,4,5,8,9,10-hexahydroanthracene (Aldrich)	HHA	C <sub>14</sub> H <sub>16</sub>	
C	9,10-dihydrophenanthrene (Aldrich)	DPh	C <sub>14</sub> H <sub>12</sub>	
C	Dibenzosuberane (Aldrich)	DBS	C <sub>15</sub> H <sub>14</sub>	
C	<i>trans</i> -perhydrofluorene (Aldrich)	<i>t</i> -PHF	C <sub>13</sub> H <sub>22</sub>	
D	4,5-dihdropyrene (TRC)	DHP	C <sub>16</sub> H <sub>12</sub>	
D	1,2,3,6,7,8-hexahdropyrene (Aldrich)	HHP	C <sub>16</sub> H <sub>16</sub>	
E	7,8,9,10-tetrahydrobenzo[a]pyrene (TRC)	THB[a]P	C <sub>20</sub> H <sub>16</sub>	
E	9H-cyclopenta[a]pyrene (TRC)	9H-Cp[a]P	C <sub>19</sub> H <sub>12</sub>	
E	4,5,7,8,10,11-hexahydro-9H-cyclopenta[a]pyrene (TRC)	HHCp[a]P	C <sub>19</sub> H <sub>18</sub>	
F	Dodecahydrotriphenylene (Aldrich)	DDHTP	C <sub>18</sub> H <sub>24</sub>	

**Table 1**  
(Continued)

Series	H <sub>n</sub> -PAH Name	Abbreviation	Formula	Structure
F	Perhydrocoronene (JCF)	PHC	C <sub>24</sub> H <sub>24</sub>	
G	5,6-dihydro-4H-benzo[de]anthracene (TRC)	DHB[de]A	C <sub>17</sub> H <sub>14</sub>	
G	4H-cyclopenta[def]phenanthrene (Aldrich)	Cp[def]Ph	C <sub>15</sub> H <sub>10</sub>	
G	11H-benzo[b]fluorene (Aldrich)	11HB[b]F	C <sub>17</sub> H <sub>12</sub>	
H	7,14-dihydrodibenz[ah]anthracene (TRC)	DHDB[ah]A	C <sub>22</sub> H <sub>16</sub>	
H	9,10-dihydrobenzo[e]pyrene (TRC)	DHB[e]P	C <sub>20</sub> H <sub>14</sub>	
H	Triptycene (Aldrich)	TRIP	C <sub>20</sub> H <sub>14</sub>	

In contrast, the spectra in this frequency region of *linear*, purely aliphatic molecules are dominated by the C–H stretching modes of H atoms bonded to aliphatic (*sp*<sup>3</sup>) C atoms present in the dominant forms of –CH<sub>2</sub>– (methylene) and –CH<sub>3</sub> (methyl) functional groups. The C–H stretching region of linear aliphatic compounds is typically dominated by four main features: the asymmetric and symmetric C–H stretching in –CH<sub>3</sub> groups, and the asymmetric and symmetric C–H stretching in –CH<sub>2</sub>– groups (Sandford et al. 1991). In the special case of *cyclic* aliphatic hydrocarbons and the aliphatic side rings on H<sub>n</sub>-PAHs, no –CH<sub>3</sub> groups are present. Thus, spectra of these materials are expected to be dominated by the asymmetric and symmetric stretching modes of methylene groups that lie near 2925 cm<sup>-1</sup> (3.419 μm) and 2850 cm<sup>-1</sup> (3.509 μm), respectively. Conveniently, these features lie at *lower* frequencies than typical of aromatic C–H stretching modes, i.e., the ranges of the C–H stretching modes of aromatics and aliphatics do not significantly overlap each other.

Conversion of a fully aromatic PAH molecule to an H<sub>n</sub>-PAH requires the addition of hydrogen atoms in even numbers in order for the molecule to remain neutral and non-radical. As a result, it is possible that the hydrogenation will incompletely convert an aromatic ring to an aliphatic one, thus disrupting

the aromatic structure, but leaving behind one or more residual double bonds. A double bond that is not part of an aromatic ring is referred to as olefinic, and will display different spectroscopic characteristics from both its aromatic and aliphatic counterparts. Specifically, the olefinic C–H stretch band appears just above 3000 cm<sup>-1</sup> (just below 3.33 μm).

In PAH molecules, the 900–650 cm<sup>-1</sup> region contains strong, typically narrow, bands caused by C–H out-of-plane (C–H<sub>OOP</sub>) bending modes (Allamandola et al. 1989b; Hudgins & Sandford 1998a, 1998b, 1998c). The frequency of an individual C–H<sub>OOP</sub> bending mode is influenced by the number of neighboring C–H units on the ring and can give important structural information about a PAH molecule. Specifically, peripheral aromatic C–H bonds fall into the following categories: solo (900–860 cm<sup>-1</sup>, 11.1–11.6 μm), duet (860–800 cm<sup>-1</sup>, 11.6–12.5 μm), trio (810–750 cm<sup>-1</sup>, 12.4–13.3 μm), and quartet (770–735 cm<sup>-1</sup>, 13.0–13.6 μm) depending on the number of adjacent C–H units on a ring (Allamandola et al. 1989b; Witteborn et al. 1989). Olefinic C–H units produce out-of-plane bending modes whose frequencies are determined by substitution patterns around the double bond. The work presented here only included *cis*-di-substituted olefins (730–665 cm<sup>-1</sup>, 13.70–15.04 μm; Silverstein & Bassler 1967).

The final spectral region, which reveals large differences between the PAH and  $H_n$ -PAH molecules, is associated with the methylene scissoring motion ( $1480\text{--}1430\text{ cm}^{-1}$ ,  $6.76\text{--}6.99\text{ }\mu\text{m}$ ; Silverstein & Bassler 1967). These are strong bands that appear only when aliphatic groups are present, are nearly constant in position, and do not strongly overlap with any strong aromatic features.

Both PAH and  $H_n$ -PAH molecules possess numerous other observable bands within the spectral region studied in this work, however, many of these bands are either weak or difficult to identify without the use of quantum calculations. Also, many of these additional bands do not provide obvious contrasts as a particular molecular skeletal structure transitions from PAH to  $H_n$ -PAH to a fully aliphatic form.

### 3.2. Conventions Used in the Figures and Band Strength Tables

Matrix isolation infrared spectra and tabular summaries of measured band positions and their relative strengths for the 23  $H_n$ -PAHs and related molecules we have studied are presented in the following text and in the Appendix. Where possible, the results are presented in series that are organized to contain molecules with related structures. For example, the first series (Series A) consists of molecules that all have the basic two-ring structure of naphthalene but that have varying amounts of excess H coverage. Series B and D (found in the Appendix) each contain several hydrogenated examples of the parent anthracene and pyrene structures, respectively. However, some series contain members that have less structural similarity, and the last series contains molecules that do not fit well into any of the previous series. In those cases where a clear sequence exists, we include some information (where available) about the fully aromatic “parent” PAH for comparison with its  $H_n$ -PAH variants. The first of these series, the  $H_n$ -naphthalenes of Series A, is presented in detail in this text, while discussion of all the other series can be found in the Appendix.

For each member within a series we provide (1) a figure that covers the portion of the infrared spectra dominated by C–H stretching vibrations (both aromatic and aliphatic) from  $3200$  to  $2700\text{ cm}^{-1}$  ( $3.125\text{--}3.704\text{ }\mu\text{m}$ ), (2) a figure that contains the remainder of the measured spectrum from  $2000$  to  $500\text{ cm}^{-1}$  ( $5.0\text{--}20\text{ }\mu\text{m}$ ), and (3) a table that summarizes the positions and relative strengths of the major absorption bands seen in each spectrum. The following conventions are used in the presentation of the data.

#### 3.2.1. Absorption Bands due to Contaminant $H_2O$

While the  $H_n$ -PAHs are responsible for the vast majority of the absorption bands seen in all the spectra, the matrices also contain low levels of background  $H_2O$ , which is the primary residual gas in our vacuum system. The main features of matrix-isolated  $H_2O$  that can be confused with  $H_n$ -PAH bands are due to H–O–H bending mode vibrations that fall in the  $1625\text{--}1590\text{ cm}^{-1}$  range, with the strongest bands near  $1624$ ,  $1608$ , and  $1593\text{ cm}^{-1}$  (Hudgins & Sandford 1998a). This same spectral region frequently also contains weak  $H_n$ -PAH fundamental and overtone/composition bands. Contaminant bands due to  $H_2O$  stretching vibrations are less of a problem since they fall to higher frequencies than the highest frequency PAH and  $H_n$ -PAH CH stretching vibrations. When clearly visible and identifiable,  $H_2O$  contaminant bands are marked with a solid dot (●) in the figures and these bands are not listed in the tables.

#### 3.2.2. Site Effects and Band Splitting

It is not uncommon for the absorption features produced by matrix-isolated species to be split or to display substructure. Such substructure commonly arises from species trapped in different matrix sites, each seeing slightly different molecular environments. This “site-splitting” is small, typically resulting in band shifts of no more than  $10\text{ cm}^{-1}$ . Matrix perturbations can also split bands simply by lifting vibrational degeneracies. In practice it can be difficult to determine whether multiple, closely spaced absorption bands are due to matrix effects or are due to distinctly different vibrational modes that happen to have similar frequencies. Therefore, multiple bands are specially noted in the tabulations shown in the Appendix. In those cases where one of the bands dominates in strength, its position is denoted with an (\*) next to the position. In those cases where there are several closely spaced bands but no obvious dominant feature, or where there is reason to believe the bands may be associated with different vibration modes, each of the band positions are specified. Bands that appear as shoulders on other, stronger bands are denoted by (sh).

#### 3.2.3. Reported Bands Strengths

Original band strengths were integrated from absorbance spectra using an algorithm provided with our spectrometer. Such integrations depend on the choice of base line for each band. Comparisons between integrations made with different choices of reasonable base lines demonstrated that the choice of base line results in variations of total band strength that were typically well below 5%, but could be higher for very weak features, particularly if these weaker bands overlap with other bands. In the worst cases, values for the weakest observable bands can be uncertain by as much as 50%.

Since we have no measure of the absolute column densities of  $H_n$ -PAHs in our samples and their intrinsic absorption band strengths are unknown, it is not possible to report absorption band strengths in absolute units. Instead, we report band strengths normalized to some dominant individual absorption band in each molecule’s spectrum. Due to the nature of  $H_n$ -PAHs, it is difficult to do the normalization in a systematic way across all the members of an  $H_n$ -PAH “family” (for example, the  $H_n$ -naphthalenes in Series A). The spectrum of a non-hydrogenated PAH is completely dominated by aromatic features, while the fully hydrogenated variant (a polycyclic aliphatic hydrocarbon) is fully dominated by a completely different set of aliphatic features. It is therefore impossible to normalize band strengths against the same band/vibrational mode across an entire “family” of  $H_n$ -PAH variants of a single PAH structure. The selection of the band against which all the other band strengths are normalized for any given molecule is therefore somewhat arbitrary. However, we have attempted to use similar bands for molecules having similar degrees of excess H coverage.

$H_n$ -PAHs, like PAHs, produce a large number of absorption bands, many of them very weak, that include both fundamental vibrations and various overtone and combination modes. We have restricted our tables to list only those bands that have strengths that exceed 5% that of the strong band to which the other bands are normalized.

#### 3.2.4. The Aromatic and Aliphatic C–H Stretching Band Complexes

The spectral structure of  $H_n$ -PAHs tends to be relatively complex in the C–H stretching region because they contain both

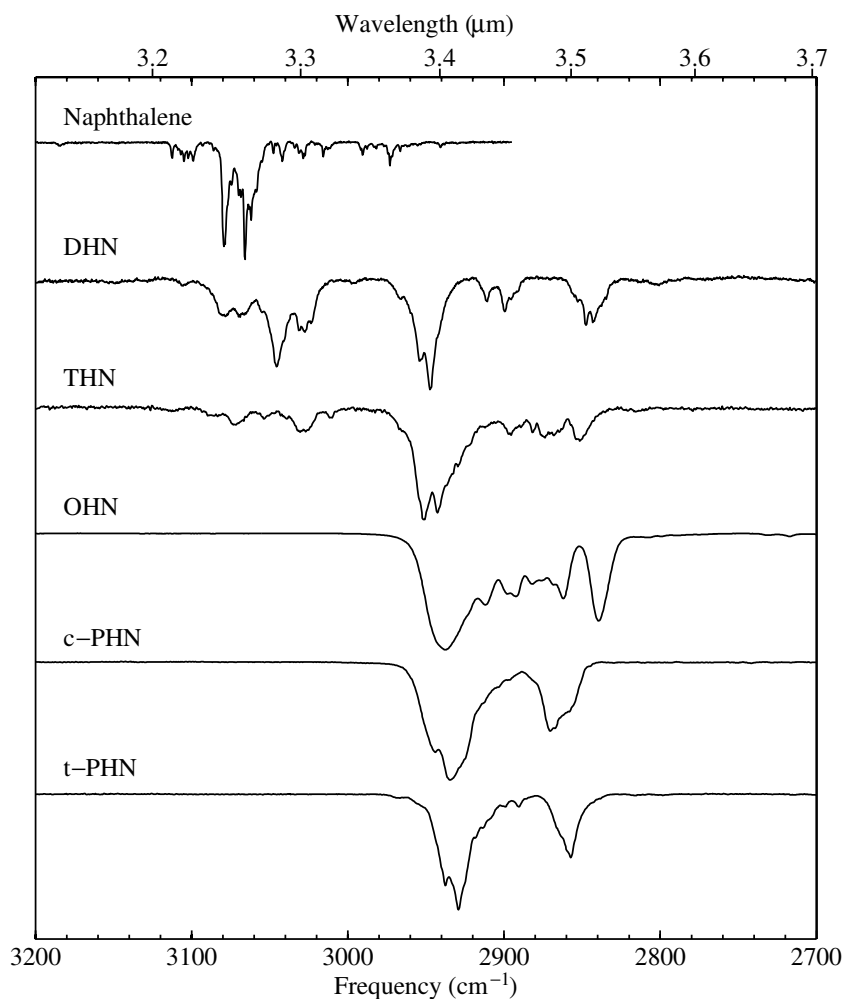


**Figure 1.** The 3200–2700  $\text{cm}^{-1}$  C–H stretch region transmission spectra of molecules in Series A (naphthalene skeletal structure). The spectrum of naphthalene is from Hudgins et al. (1994).

aromatic and aliphatic C–H bonds and frequently each of these resides in a variety of different structural sites. This results in bands that typically separate well into aromatic and aliphatic groups, but individual bands typically overlap within these two groups. Where such overlaps occur, we provide a frequency range over which the total band area has integrated (typically the entire aromatic or aliphatic C–H stretching region), followed by the area of the combined bands in that range. The positions of specific band peaks within that range are then listed on the lines below.

### 3.3. Description of Results

In the section below we provide a complete discussion of the results for those molecules falling in Series A, i.e., the  $\text{H}_n$ -naphthalenes. Similar discussions can be found in the Appendix for each of the members of the other series shown in Table 1.

#### 3.3.1. Series A (Naphthalene, DHN, THN, OHN, c-PHN, t-PHN):

The 3200–2700 and 2000–500  $\text{cm}^{-1}$  spectra of matrix isolated naphthalene and  $\text{H}_n$ -PAHs with a naphthalene skeletal structure are presented in Figures 1 and 2, respectively. The spectrum of the PAH naphthalene appears at the top of each figure and H coverage increases downward until the bottom where the last two molecules are fully (hydrogenated) versions of naphthalene ( $\text{C}_{10}\text{H}_{20}$ ). The positions and relative strengths of

absorption bands seen in the spectra of these molecules are listed in Tables 2–6. The C–H stretching region of many of these  $\text{H}_n$ -PAHs has previously been examined in Bernstein et al. (1996).

The 3200–2700  $\text{cm}^{-1}$  spectra in Figure 1 contain the C–H stretch bands for all of these molecules. Fully aromatic naphthalene displays the characteristic aromatic C–H stretch bands (Wexler 1967; Hudgins et al. 1994; Hudgins & Sandford 1989a) whose main features appear between 3093–3049 and 3118–3093  $\text{cm}^{-1}$  with no other significant bands except for some weaker overtones/combinations of lower frequency modes. The change from fully aromatic naphthalene to dihydronaphthalene (DHN;  $\text{H}_2$ -naphthalene) is marked by a shift and broadening of the aromatic C–H stretch bands, spanning 3097–3009  $\text{cm}^{-1}$ . Additionally, a large aliphatic C–H stretch feature (Wexler 1967) with several complex series of bands centered near 2950, 2905, and 2845  $\text{cm}^{-1}$  emerges, corresponding to the two new  $\text{CH}_2$  groups. The aromatic features of tetrahydronaphthalene (THN;  $\text{H}_4$ -naphthalene) span the same range as those seen in DHN, however, the aliphatic features are considerably stronger, more complex, and more overlapping, and now span the whole range from 2990 to 2801  $\text{cm}^{-1}$ . The rest of the molecules in this series no longer have doubly bonded carbon-bearing hydrogen atoms, so aromatic C–H stretches are no longer present. Only aliphatic C–H stretch bands remain at 2980–2818, 2979–2888, and 2974–2878  $\text{cm}^{-1}$  for octahydronaphthalene (OHN;  $\text{H}_8$ -naphthalene), and the two

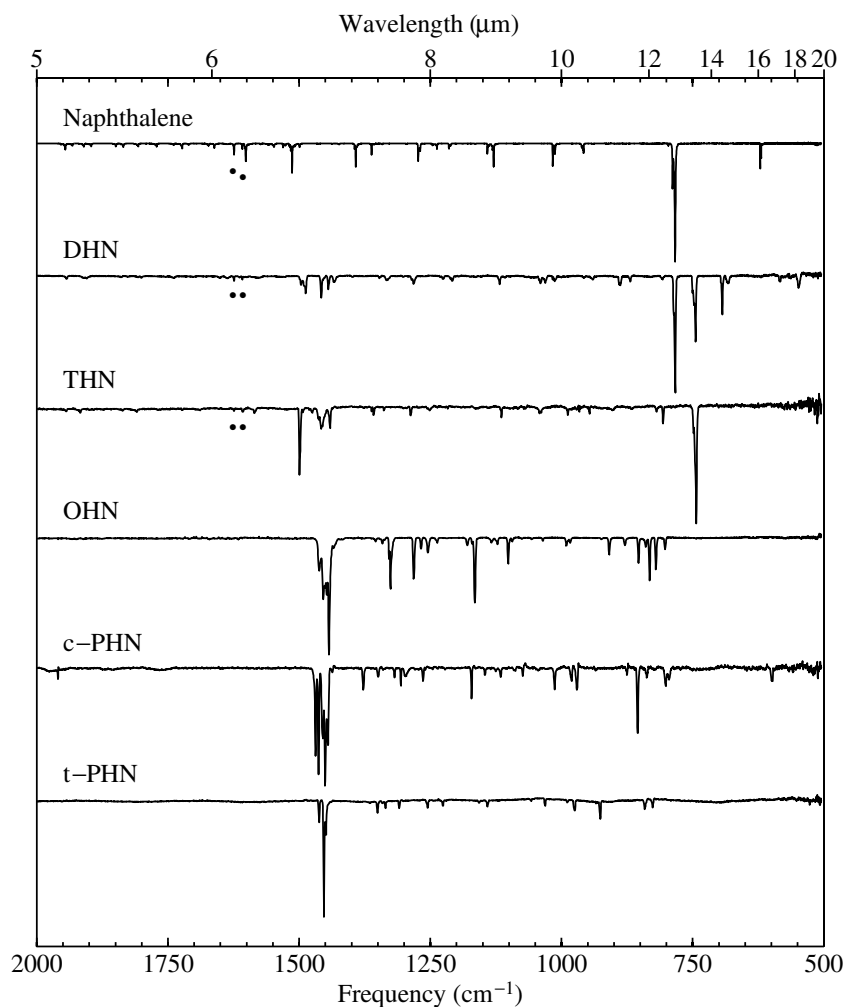


**Figure 2.** The 2000–500  $\text{cm}^{-1}$  spectral region transmission spectra of molecules in Series A (naphthalene skeletal structure). The spectrum of naphthalene is from Hudgins et al. (1994). A (\*) denotes bands due to trace  $\text{H}_2\text{O}$  contamination.

decahydronaphthalenes ( $\text{H}_{10}$ -naphthalene *c*-PHN, and *t*-PHN), respectively.

The 2000–500  $\text{cm}^{-1}$  spectra in Figure 2 contain many bands, some of which cannot be definitively assigned to specific vibrational motions without extensive theoretical calculations. Nonetheless, we can make some general observations about the types of bands observed. Naphthalene possesses aromatic carbon deformation modes at 619.4  $\text{cm}^{-1}$  and 621.4  $\text{cm}^{-1}$ . These features disappear in all subsequent members of this series. Naphthalene possesses a strong pair of bands near 785  $\text{cm}^{-1}$  associated with quartet C–H out-of-plane bending ( $\text{C-H}_{\text{OOP}}$ ) modes (Wexler 1967; Allamandola et al. 1989b; Witteborn et al. 1989). In DHN, the same bands appear near 785  $\text{cm}^{-1}$ . Additionally, DHN possesses a series of three bands near 747  $\text{cm}^{-1}$ , as well as bands at 693.3 and 682.2  $\text{cm}^{-1}$  that may represent quartet aromatic and olefinic C– $\text{H}_{\text{OOP}}$  bending (Silverstein & Bassler 1967). In THN, there is only one large quartet C– $\text{H}_{\text{OOP}}$  bending feature consisting of a pair of bands near 745  $\text{cm}^{-1}$ . All subsequent members of this series have had their aromaticity destroyed by hydrogenation and their spectra lack this bend. The spectrum of naphthalene possesses bands from 1600 to 1000  $\text{cm}^{-1}$  that are attributed to the C–H in-plane bending and aromatic carbon skeletal stretching (Silverstein & Bassler 1967). This region is also populated by overtones and combinations of lower frequency modes. As the aromaticity is decreased and the carbon rings become

more flexible, a series of bands from 1480 to 1430  $\text{cm}^{-1}$  associated with methylene scissoring (Wexler 1967) appear. Additionally, as the aromaticity is broken down, aromatic skeletal stretching and C–H in-plane bending bands are replaced by C–C skeletal vibrations (1200–800  $\text{cm}^{-1}$ ) and methylene twisting and wagging (1350–1150  $\text{cm}^{-1}$ ) (Silverstein & Bassler 1967).

Spectra of molecules containing aromatic domains often show a number of weak features in the 1950–1850  $\text{cm}^{-1}$  region due to overtones of the strong aromatic C– $\text{H}_{\text{OOP}}$  modes (Allamandola et al. 1989a; Hudgins & Sandford 1989a, 1989b, 1989c). Spectra of many of the  $\text{H}_n$ -PAHs also contain absorption bands in this region, although they are frequently too weak to meet the threshold requirement to be listed in the tables.

Again, the Appendix contains similar discussions, figures, and tables for the  $\text{H}_n$ -PAHs belonging to the other series shown in Table 1.

#### 3.4. Discussion of Laboratory Results: *H<sub>n</sub>-PAH Spectral Patterns*

Hydrogenation of PAH molecules causes significant and ubiquitous changes in the mid-IR spectra of these molecules when compared with the original PAH. We will address these differences in separate sections associated with different chemical bonds found in these molecules.

**Table 2**  
1,2-dihydronaphthalene (DHN)

Band Position (cm <sup>-1</sup> )	Normalized Band Area
548.1	0.15
583.4	0.05
682.2	0.11
693.3	0.24
744.1*, 747.3, 749.9	0.70
783.0*, 785.8	<b>1.00</b>
887.4, 889.9	0.11
939.3	0.05
1012.6*, 1016.4	0.09
1030.7	0.06
1042.5, 1039.8*	0.07
1117.5	0.05
1211.0, 1207.6*	0.06
1285.0, 1281.5*	0.11
1332.8	0.07
1432.9	0.08
1444.1	0.10
1457.5	0.21
(1502–1483): 1498.4, 1496.1, 1490.0, 1487.1*	0.33
(1546–1514): 1539.5, 1526.5*, 1518.2	0.07
1589.1, 1575.7*	0.07
2800.9	0.08
2846.4, 2841.9	0.39
2910.2, 2898.6	0.25
2965.4, 2952.3, 2946.2*	1.05
(3097–3009): 3078.4*, 066.5*, 3054.0, 3044.5*, 3029.9, 3026.6*, 3022.3	1.51

**Table 3**  
1,2,3,4-tetrahydronaphthalene (THN)

Band Position (cm <sup>-1</sup> )	Normalized Band Area
748.1, 742.9*	<b>1.00</b>
806.1	0.07
1287.1	0.05
1440.7	0.12
(1469–1446): 1462.6, 1457.7*, 1455.2, 1450.6	0.35
1499.0*, 1492.6	0.40
(2990–2801): 2950.3*, 2941.4*, 2895.1, 2880.6, 2869.1, 2850.7, 2814.3	4.76
(3124–2997): 3111.5, 3086.1, 3071.2*, 3052.4, 3038.6, 3027.5*, 3009.8	0.78

### 3.4.1. C–H Stretching Vibration Modes

Some of the strongest features of the spectra of PAH molecules appear in the C–H stretch region. In regular PAHs, this region is dominated by aromatic C–H stretching modes that

**Table 4**  
1,2,3,4,5,6,7,8-octahydronaphthalene (OHN)

Band Position (cm <sup>-1</sup> )	Normalized Band Area
819.8	0.07
831.7	0.08
852.8	0.07
1101.1	0.06
1169.8, 1164.7*	0.17
1254.4	0.05
1281.2	0.11
1328.0, 1325.4*	0.16
(1471–1425): 1461.4, 1453.6, 1450.1, 1447.0, 1442.7*, 1434.0	<b>1.00</b>
(2693–2647): 2682(sh), 2676.1, 2667.0*, 2660.0	0.21
(2741–2693): 2730.1, 2716.0*, 2697.8	0.08
(2980–2818): 2936.6*, 2911.1, 2896.9, 2891.8, 2881.1, 2875.1, 2867.3, 2861.3, 2838.6*	20.67

**Table 5**  
*cis*-decahydronaphthalene (*c*-PHN)

Band Position (cm <sup>-1</sup> )	Normalized Band Area
598.7	0.05
801.1, 794.5	0.06
854.5	0.17
980.8, 970.2	0.25
1171.1	0.05
1377.3	0.05
1454.4, 1450.0*, 1444.7	<b>1.00</b>
1462.7	0.25
1468.4	0.24
(2888–2839): 2867.8*, 2858(sh)	6.68
(2979–2888): 2932.1*, 2943.1	19.25

typically fall in the 3200–3000 cm<sup>-1</sup> (3.13–3.33 μm) range. As the molecule becomes hydrogenated, aromatic (*sp*<sup>2</sup>) carbons are converted to aliphatic (*sp*<sup>3</sup>) carbons and the aliphatic C–H stretch bands of –CH<sub>2</sub>– groups (methylene) begin to appear in the 3000–2700 cm<sup>-1</sup> range (3.33–3.70 μm) while the original aromatic bands are weakened. The strength of these aliphatic bands grows quickly relative to the aromatic bands. One of the reasons for this is that each aliphatic methylene group has two C–H stretches where there would be only one C–H stretch if the carbon were aromatic. Additionally, the intrinsic absorption strength of an aliphatic C–H stretching vibration is typically two to three times stronger per bond than the intrinsic strength of an aromatic mode (Wexler 1967). As a result, as additional H atoms are incorporated into the molecule, the intensities of the aliphatic C–H stretch features quickly grow to match, and subsequently dwarf, the original aromatic features. This effect is easily seen in, for example, series A, B, and D (Figures 1, 9, and 13), each of which starts with the same basic PAH skeleton

**Table 6**  
*trans*-decahydronaphthalene (*t*-PHN)

Band Position ( $\text{cm}^{-1}$ )	Normalized Band Area
826.0	0.08
841.3	0.11
925.6	0.13
974.4	0.10
1030.9	0.05
1140.6	0.06
1254.7	0.06
1308.9	0.06
1350.1	0.08
1452.2*, 1448.5	<b>1.00</b>
1461.5	0.15
2671.1, 2665.6	0.14
2801.0, 2797.2	0.05
2815.4	0.05
2856.4	5.67
(2974–2878): 2967.6, 2936.4, 2928.2*, 2919(sh), 2913(sh), 2899.5, 2890.7	22.90

and leads to progressively more hydrogenated versions of the initial molecule.

Using series A as an example (Figure 1), we start with a fully aromatic naphthalene skeleton, which possesses eight aromatic hydrogens. The second member of this series, DHN, which is naphthalene twice hydrogenated, has four aromatic hydrogens, two olefinic hydrogens (whose bands appear mixed with the aromatic bands), and four aliphatic hydrogens. Despite the fact that the combined olefinic and aromatic hydrogens outnumber their aliphatic counterparts by a 3:2 ratio, the integrated intensities of their bands are only about 85% as strong as those arising from the four aliphatic C–H bonds. Similarly, in THN, with its four extra H atoms, there are four aromatic and eight aliphatic hydrogens, yet the integrated intensities of the aromatic C–H stretch bands are only about 16% of the strength of the aliphatic C–H stretch bands. Even a modest level of hydrogenation can result in major changes in the profiles and strengths of the C–H stretching modes of these molecules and the appearance of significant bands associated with aliphatic C–H stretching. It also follows that even a modest concentration of  $H_n$ -PAHs can have a significant effect on the overall spectrum of a mixture of PAHs and  $H_n$ -PAHs in this spectral region.

#### 3.4.2. C–H Out-of-plane (C–H<sub>oop</sub>) Modes

The C–H<sub>oop</sub> bending region provides important structural information about both PAH and  $H_n$ -PAH molecules. First, hydrogenation disrupts the aromaticity of the ring to which the H atom is added and can totally eliminate some of the defining bands of the original PAHs. It is not just the number of additional hydrogen atoms, but where they lie that determines the spectrum. For example, anthracene has two isolated aromatic C–H bonds on the central rings and four aromatic C–H bonds on the two end rings, and its spectrum shows distinct bands associated with each at 878 and 728  $\text{cm}^{-1}$  (11.4 and 13.7  $\mu\text{m}$ ), respectively (Figure 10). However, DHA has lost the solo band to hydrogenation of the central carbons, leaving the quartet bands,

corresponding to the undisturbed sets of four hydrogen atoms on the end rings. Similarly, in HHP, the trio bands usually seen in pyrene at 712 and 745  $\text{cm}^{-1}$  (14.0 and 13.4  $\mu\text{m}$ ) are missing (Figure 14) because the two rings that bore three C–Hs have been reduced to CH<sub>2</sub> groups. In the extreme case of DDHTP, the aromaticity of the central ring has been preserved, but all bands associated with the C–H<sub>oop</sub> bending mode are absent (Figure 18).

Second, partial hydrogenation of a ring may leave behind residual olefinic CH units and new C–H<sub>oop</sub> bending modes associated with these groups appear. For example, naphthalene has two identical rings each with four aromatic C–Hs resulting in a pair of bands near 785  $\text{cm}^{-1}$  (12.7  $\mu\text{m}$ ) associated with quartet C–H out-of-plane bending (C–H<sub>oop</sub>) (Figure 2). The addition of two hydrogen atoms to one of those rings introduces two CH<sub>2</sub> groups to that ring, but leaves two C–H bonds, which are olefinic rather than aromatic and this changes the absorption features due to these two C–H bonds. The addition of two more hydrogen atoms to the same ring (THN) leaves one ring of aliphatic CH<sub>2</sub> groups and one aromatic ring of C–Hs that produce a quartet C–H<sub>oop</sub> features near 745  $\text{cm}^{-1}$  (13.4  $\mu\text{m}$ ). Had the second pair of hydrogen atoms been added to the other ring it would still be an H<sub>4</sub>-naphthalene, but the result would have been two rings having a mixture of C–H and CH<sub>2</sub> groups. Olefinic C–H<sub>oop</sub> modes typically appear from 980 to 960  $\text{cm}^{-1}$  (10.2–10.4  $\mu\text{m}$ ) for *trans*-hydrogens, and from 730 to 665  $\text{cm}^{-1}$  (13.7–15.0  $\mu\text{m}$ ) for *cis*-hydrogens (Silverstein & Bassler 1967). Because we have limited ourselves to ring structures only, all of the olefinic units presented in this paper have *cis*-hydrogens and thus appear in the 730–665  $\text{cm}^{-1}$  (13.7–15.0  $\mu\text{m}$ ) region. This falls mostly outside the normal range for aromatic C–H<sub>oop</sub> bending modes, though occasionally it will overlap with carbon skeletal deformation modes. Examples of olefinic C–H<sub>oop</sub> bending modes can be seen in DHN (Figure 2; 693.3 and 682.2  $\text{cm}^{-1}$ ), HHA (Figure 10; 655.6  $\text{cm}^{-1}$ ), 9H-Cp[a]P (Figure 16; 674.7  $\text{cm}^{-1}$ ), and DHB[e]P (Figure 22; 674.9  $\text{cm}^{-1}$ ).

Finally, hydrogenation can break the degeneracy of modes that were equivalent in the parent PAH molecule, and this can lead to more complicated spectra. The degeneracy can be broken in two ways.

First, an aromatic C–H unit whose next nearest neighbor is a methylene unit is not equivalent to one whose next nearest neighbor is another aromatic C–H unit. The differences in the local electronic structure, the strain created by the aliphatic  $sp^3$  bonding that no longer allows the carbon atoms to lie in a flat planar structure, and the steric hindrance from extra hydrogens can lead to differences in the infrared spectra. This effect may be the cause for the pattern observed in the Series A (naphthalene skeletal structure) C–H<sub>oop</sub> bend mode bands. In normal naphthalene, the quartet bands of both rings appear as one major feature around 785.0  $\text{cm}^{-1}$  (12.74  $\mu\text{m}$ ), while in DHN, where the aromatic C–H units are no longer equivalent, they appear around 784 and 747  $\text{cm}^{-1}$  (12.8 and 13.4  $\mu\text{m}$ ) (Figure 2).

Second, the degeneracy can also be broken because the aliphatic portion of a ring, in combination with surface effects, may be able to adopt multiple different conformations and cause a loss of chemical equivalence. This effect may be the cause for the C–H<sub>oop</sub> bend pattern seen in the spectra of molecules in series C. The aromatic C–H<sub>oop</sub> duet band seen in phenanthrene (Figure 12) at 813  $\text{cm}^{-1}$  (12.3) are removed by hydrogenation in DHPH, but the main quartet band around 746  $\text{cm}^{-1}$  (13.4  $\mu\text{m}$ ) and possibly a small quartet band around 774  $\text{cm}^{-1}$  (12.9  $\mu\text{m}$ )

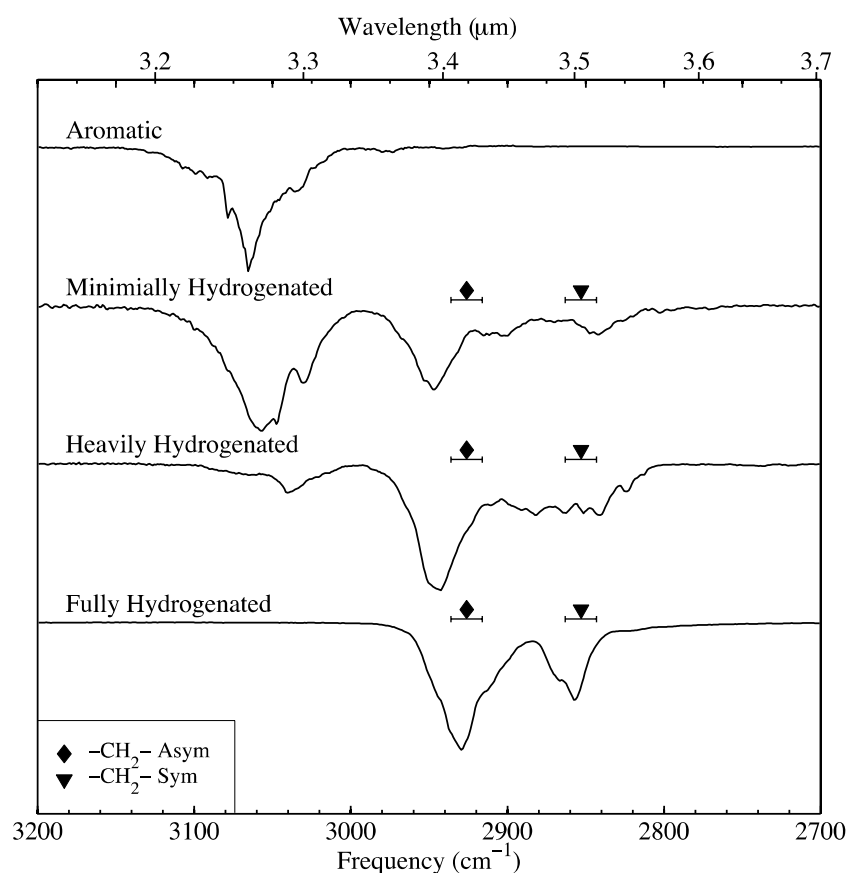


**Figure 3.** The 3200–2700  $\text{cm}^{-1}$  CH stretch region transmission spectra of co-added groups of molecules ranging from fully aromatic (top) to fully aliphatic (bottom). The transition from features due solely to aromatic C–H groups to features due solely to aliphatic asymmetric and symmetric stretching in  $-\text{CH}_2-$  groups is readily apparent. Canonical ranges for the  $-\text{CH}_2-$  asymmetric and symmetric stretches in an alkane are shown by the bars and denoted by a diamond and triangle, respectively.

remain (Figure 12). In this case, the groups neighboring the two aromatic rings are identical; however, they can adopt two possible doubly degenerate conformations, namely, a half boat or a half chair structure. Of these, the chair is highly favored because of strain, which may account for some of the difference in observed band strengths. The next molecule in the series is DBS, which has an additional methylene unit and can adopt additional conformations. The spectrum of DBS has three large  $\text{C-H}_{\text{OOP}}$  features that appear around 762, 750, and 738  $\text{cm}^{-1}$  (13.1, 13.3, and 13.6  $\mu\text{m}$ ) (Figure 12). Finally, fluorene has one methylene unit, which can only adopt one degenerate pair of conformations. This is supported by the spectrum of fluorene, which only has one the  $\text{C-H}_{\text{OOP}}$  bending band at 740  $\text{cm}^{-1}$  (13.5  $\mu\text{m}$ ) (Figure 12).

#### 3.4.3. C–H In-plane and Multiple C–C Modes in the 2000–1000 $\text{cm}^{-1}$ (5–10 $\mu\text{m}$ ) Range

Without the help of quantum calculations it is difficult to make precise assignments for absorptions between 2000 and 1000  $\text{cm}^{-1}$  in many of the spectra of  $H_n$ -PAHs. The region between roughly 1480 and 1430  $\text{cm}^{-1}$  (6.76–6.99  $\mu\text{m}$ ) is mostly unremarkable in regular PAH molecules, but  $H_n$ -PAH molecules possess strong bands associated with methylene scissoring at this location. These bands appear in the spectra of *all*  $H_n$ -PAHs, in roughly the same range, largely independent of skeletal structure. As a result, *the methylene scissoring feature represents a strong diagnostic of the presence of  $H_n$ -PAHs as a class.* As the level of hydrogenation increases, the strength of these bands increases to the point where they approach the  $\text{C-H}_{\text{OOP}}$  bending modes in intensity. It is interesting to note

the reduction in the complexity of these bands in *t*-PHN with respect to *c*-PHN (Figure 2), despite the fact that *t*-PHN and *c*-PHN are both  $\text{C}_{10}\text{H}_{18}$ . This may be caused by *t*-PHN's  $C_{2h}$  symmetry as well as its rigid structure which cannot interconvert between chair forms in the two cyclohexane rings. In contrast, *c*-PHN is sterically strained but able to interconvert between chair forms of each of the two cyclohexane rings, which creates more chemically inequivalent hydrogens, leading to additional spectral complexity (Quinkert et al. 1996). Thus, the 1480–1430  $\text{cm}^{-1}$  (6.76–6.99  $\mu\text{m}$ ) region is both diagnostic of hydrogen coverage and can provide information about structural details of the molecule.

#### 3.4.4. The General Spectral Behavior of the PAH $\rightarrow H_n$ -PAH Transition

While the various molecules discussed in this paper have a wide variety of structures, and therefore produce unique and complex infrared spectra, they all manifest a common set of spectral changes as fully aromatic molecules are sequentially hydrogenated. Examples of this transition are best demonstrated by the spectra of the molecules in Series A (naphthalenes and  $H_n$ -naphthalenes) seen in Figures 1 and 2, but the general behavior of this evolution is seen in all the molecules we have examined, independent of the structures of the molecules involved. The basics of these changes are demonstrated in Figures 3 and 4, in which we have co-added the spectra shown earlier into four groups: (1) fully aromatic (naphthalene, anthracene, phenanthrene, pyrene, B[e]P, B[a]P, coronene, triphenylene), (2) minimally hydrogenated (DHN, DHA, DHPH, fluorene, DHP, Cp[def]Ph, 11HB[b]F, DHB[e]P, DHB[a]P,

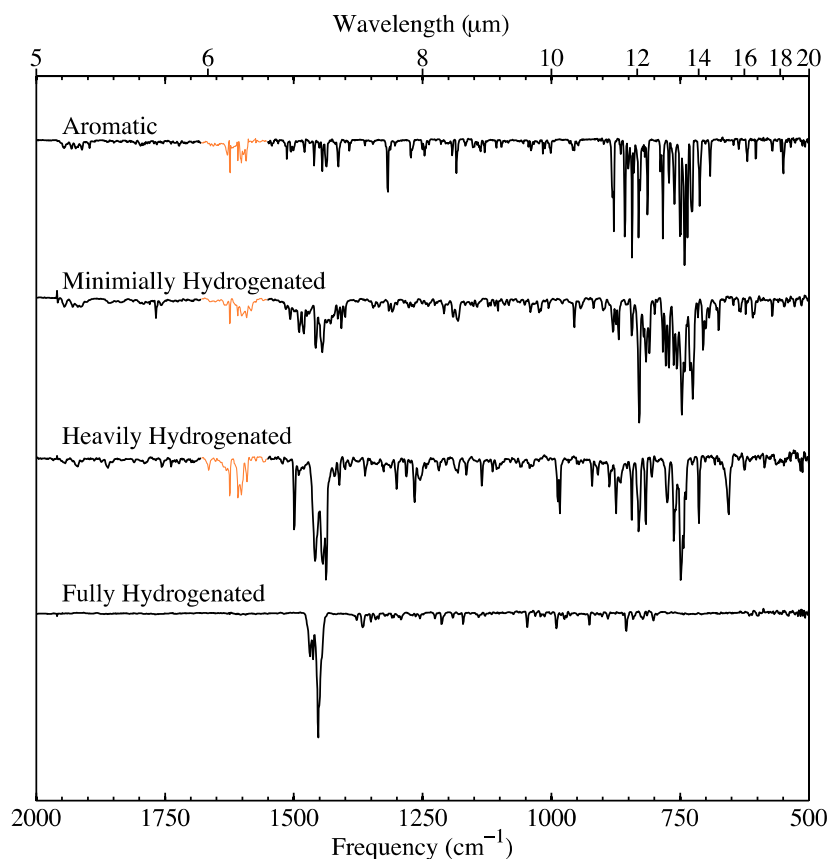


**Figure 4.** The 2000–500  $\text{cm}^{-1}$  transmission spectra of co-added groups of molecules ranging from fully aromatic (top) to fully aliphatic (bottom). These are associated with the same spectral co-adds shown in Figure 3. The highlighted region contains bands that may in part be due to  $\text{H}_2\text{O}$  contamination.

(A color version of this figure is available in the online journal.)

9H-Cp[a]P, DHDB[ah]A), (3) heavily hydrogenated (THN, OHN, HHA, DBS, HHP, DHB[de]A, DDHTP, THB[a]P, HHCp[a]P), and (4) fully hydrogenated (*c*-PHN, *t*-PHN, *t*-PHF, PHC). The category of minimally hydrogenated is defined as either having the minimum allowed number of hydrogens added to the parent PAH molecule without creating a radical or ion or a molecule containing a five-member ring that cannot be aromatic in its neutral form. The heavily hydrogenated category consists of all remaining hydrogenated molecules that are more than minimally hydrogenated, but not fully aliphatic. To create these plots, each initial spectrum was normalized so that the tallest peak in the plotted range was 1 unit in height (i.e., the co-additions do not necessarily represent equal column densities of each molecule). Subsequently, the spectra were co-added and the spectral sums were normalized again so that the tallest peak in the plotted range of each composite spectrum was 1 unit in height. Bands located within the sections of the spectra that are highlighted are located in regions where features associated with matrix-isolated water have been subtracted from the composite spectra. Since this subtraction process is not perfect, residual bands in this region should be considered with caution.

These figures show the same general trend seen for specific families as the naphthalene sequence seen in Series A (Figures 1 and 2). In particular, the conversion from fully aromatic PAHs to fully hydrogenated cyclic aliphatics produces two large and characteristic spectral changes. First, in the C–H stretching region, the addition of H atoms results in a steady transition from bands in the 3100–3000  $\text{cm}^{-1}$  (3.23–3.33  $\mu\text{m}$ ) range due to the stretching of aromatic C–H groups to features due solely to aliphatic stretching in  $-\text{CH}_2-$  groups. The aliphatic

C–H stretch features can be subdivided into symmetric and asymmetric modes whose canonical positions, 2863–2843  $\text{cm}^{-1}$  (3.49–3.52  $\mu\text{m}$ ) and 2936–2916  $\text{cm}^{-1}$  (3.41–3.43  $\mu\text{m}$ ), respectively, are denoted in Figure 3. It should be noted that the collective spectra of fully hydrogenated molecules most closely match the canonical aliphatic values because they contain little of the additional strain of neighboring aromatic or olefinic moieties that cause these bands to be blueshifted in the partially hydrogenated variants (Silverstein & Bassler 1967). At lower frequencies, the most obvious effects of H addition are the decline in the intensity of bands in the C–H<sub>OOP</sub> region and the growing strength of the methylene scissoring feature between 1480 and 1430  $\text{cm}^{-1}$  (6.76–6.99  $\mu\text{m}$ ). Regular neutral PAH molecules typically only show weak features in this region, but in fully hydrogenated molecules this band dominates the entire 2000–500  $\text{cm}^{-1}$  (5–20  $\mu\text{m}$ ) spectral region.

#### 4. IMPLICATIONS FOR ASTROPHYSICS

There have been a variety of hypotheses suggested as sources of the emission features that fall in the 3.4–3.6  $\mu\text{m}$  range that typically accompany the stronger PAH emission feature near 3.3  $\mu\text{m}$ . These sources include overtones and combinations of lower frequency PAH vibrational modes and “hot” bands associated with relaxation of higher anharmonic vibrational modes of the aromatic C–H stretch (Barker et al. 1987; Allamandola et al. 1989b), C–H stretching vibrations from aliphatic side groups on PAHs (Jourdain de Muizon et al. 1990; Sandford 1991), and the C–H stretching vibrations of  $\text{H}_n$ -PAHs (Bernstein et al. 1996; Sloan et al. 1997). While it is quite likely that a combination of

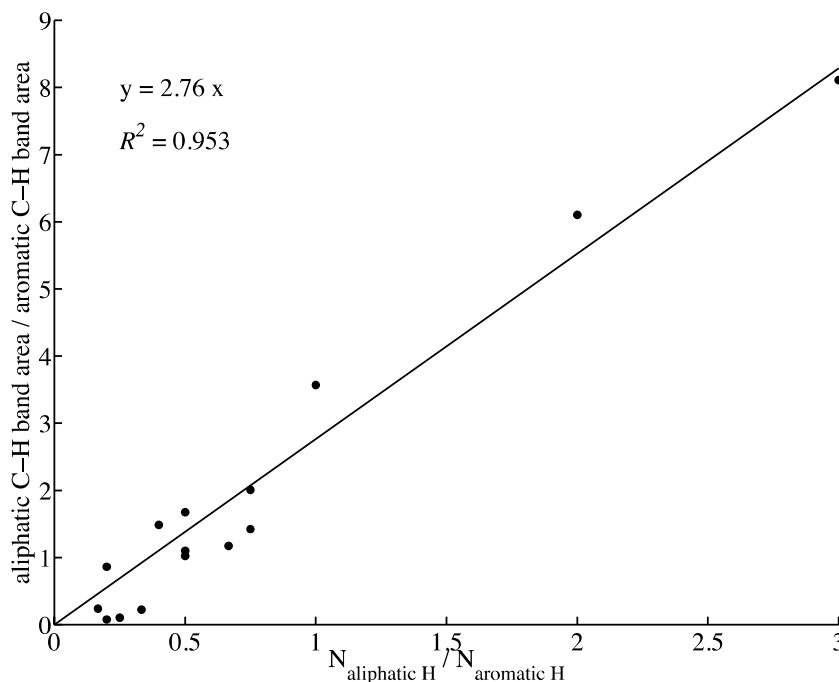


**Figure 5.** The ratios of integrated band areas ( $\text{cm}^{-1}$ ) of aliphatic C–H stretching vs. both aromatic and olefinic C–H stretching features compared to the actual numerical quantity of aliphatic vs. aromatic plus olefinic C–H bonds for  $H_n$ -PAH molecules. Fully aromatic, fully aliphatic, and HHA (which contains no aromatic bands) have been excluded from the plot.

these sources contributes to the emission seen in the  $3.4\text{--}3.6\ \mu\text{m}$  region, and that the relative contribution of these sources may vary from object to object, for the purposes of the discussion that follows, we will assume that all of the emission comes from  $H_n$ -PAHs. Making this assumption means that we are very likely overestimating the true contribution of  $H_n$ -PAHs to a given emission spectrum and any constraints placed on relative abundances of these materials should be considered to be upper limits.

#### 4.1. The C–H Stretch Region ( $3.3$ and $3.4\text{--}3.6\ \mu\text{m}$ Features)

The ratios of the relative integrated band strengths of the aliphatic (appearing at  $3.4\ \mu\text{m}$ ) versus aromatic and olefinic (appearing at  $3.3\ \mu\text{m}$ ) C–H stretch features in the laboratory data are proportional to the quantity of aliphatic versus aromatic and olefinic C–H bonds present in each molecule. This relationship, illustrated in Figure 5, can be used to compute upper limits on excess hydrogenation of PAHs in astronomical objects. The slope of the line fit to the data in Figure 5 is 2.76, which is entirely consistent with the relative intrinsic strengths of typical aliphatic and aromatic C–H bonds (Wexler 1967). It should be noted that the actual numeric value of the ratio of integrated  $3.3$  and  $3.4\ \mu\text{m}$  band strengths are dependent on the choice of units,  $\text{cm}^{-1}$  or  $\mu\text{m}$  (we chose  $\text{cm}^{-1}$ ), but the resulting estimated upper limits of C–H to  $\text{CH}_2$  groups remains the same in either case. It should also be noted that this analysis does not specify the distribution of any hydrogenation. Specifically, it does not specify whether the excess hydrogen is spread out among the entire population of PAH molecules, or whether there is a subset of molecules that are highly hydrogenated while others remain completely or largely in the form of normal aromatic PAHs.

Figure 6 contains spectra showing the  $3200\text{--}2700\ \text{cm}^{-1}$  region of three celestial objects: IRAS 21282+5050, a planetary nebula with “normal” PAH emission bands, and IRAS 22272+5435 and IRAS 04296+3429, which are protoplanetary

nebulae with abnormally large  $3.4\ \mu\text{m}$  features. The ratios of the integrated band strengths for the aliphatic ( $3.4\ \mu\text{m}$ ) versus aromatic ( $3.3\ \mu\text{m}$ ) features (with band areas integrated in  $\text{cm}^{-1}$ ) are  $\sim 0.44$ ,  $\sim 1.3$ , and  $\sim 1.8$  for IRAS 21282+5050, IRAS 22272+5435, and IRAS 04296+3429, respectively. If we compare these integrated band strengths to those observed in our laboratory absorption data, and assume  $H_n$ -PAHs are responsible for everything seen at  $3.4\ \mu\text{m}$ , we can derive an estimated ratio of the total number of cyclic aliphatic hydrogens relative to aromatic hydrogens along the line of sight to each object. The resulting ratios of  $N_{\text{aliphatic H}}/N_{\text{aromatic H}}$  are 0.16, 0.47, and 0.65 for IRAS 21282+5050, IRAS 22272+5435, and IRAS 04296+3429, respectively. *These results suggest that aromatic C–H moieties outnumber aliphatic C–H bands in each of the objects, even in those objects with anomalously stronger  $3.4$  features.*

It should be noted that the emission bands near  $3.4\ \mu\text{m}$  in these objects fall at locations that are slightly blueshifted from the canonical values of the asymmetric C–H stretch of aliphatic  $-\text{CH}_2-$  groups (Figure 6), consistent with  $-\text{CH}_2-$  residing near strained rings like those in our minimally to heavily hydrogenated  $H_n$ -PAHs (see Figure 3). We also note that the spectra of these objects do not contain any feature at the canonical location of the strong aliphatic  $-\text{CH}_3$  asymmetric stretch near  $2965\ \text{cm}^{-1}$  (Figure 6). The  $-\text{CH}_3$  and  $-\text{CH}_2-$  symmetric stretches that fall at longer wavelengths (see Figure 6) often blend in molecules having mixed chemical moieties (Sandford et al. 1991), making it difficult to use them to place any additional limits on the presence of  $-\text{CH}_3$  side groups. Overall, the data are more consistent with the presence of cyclic aliphatics or  $H_n$ -PAH molecules than with pure aliphatics or PAHs with aliphatic side chains containing  $-\text{CH}_3$  termini. Thus, *minimally to heavily hydrogenated  $H_n$ -PAHs could represent a significant contributing factor to the infrared spectra of these objects*, particularly in those objects with anomalously strong features near  $3.4\ \mu\text{m}$ . However, it is worth reiterating that, overall, the number of implied aromatic C–H groups dominates

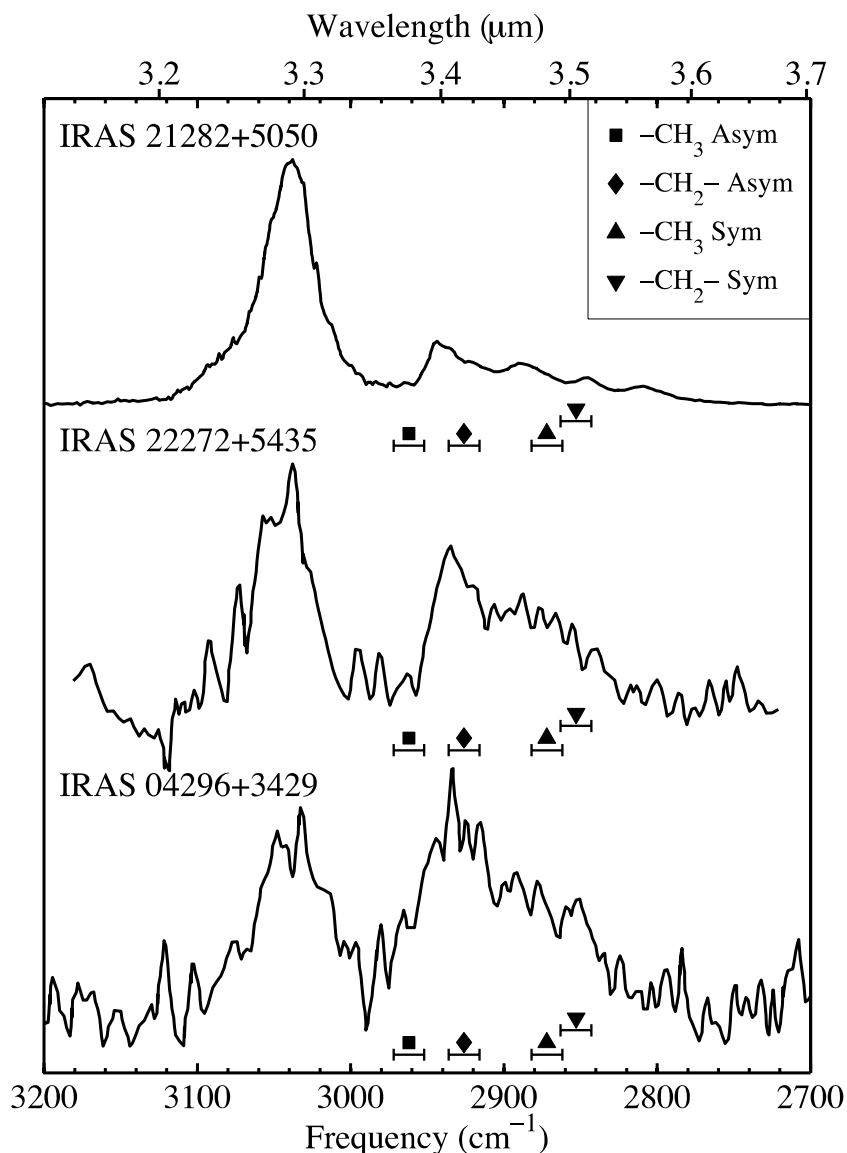


**Figure 6.** Spectra of a normal PAH emitter (IRAS 21282+5050) and two objects with abnormally strong  $3.4\ \mu\text{m}$  features (IRAS 22272+5435 and IRAS 04296+3429). The spectrum of IRAS 21282+5050 is taken from Jourdain de Muizon et al. (1986) and the spectra of IRAS 22272+5435 and IRAS 04296+3429 are taken from Geballe et al. (1992). Underlying continua have been removed for each object. The canonical positions of the aliphatic  $-\text{CH}_3$  and  $-\text{CH}_2-$  asymmetric and symmetric stretches are denoted.

over the number of aliphatic groups, even for those objects with anomalously strong  $3.4\ \mu\text{m}$  features.

#### 4.2. The Methylene Scissoring Region ( $6.9\ \mu\text{m}$ Feature)

In addition to the C–H stretch features, our laboratory data show that  $\text{H}_n$ -PAHs also produce characteristic methylene scissoring features near  $1450\ \text{cm}^{-1}$  ( $6.9\ \mu\text{m}$ ) due to C atoms having excess hydrogenation at the periphery of the molecule. Our laboratory data therefore suggest that if C–H stretching in  $\text{H}_n$ -PAH molecules is responsible for a portion of the  $3.4\ \mu\text{m}$  features observed in the spectra of a variety of celestial objects, there should be accompanying features at  $6.9\ \mu\text{m}$ .

This observation is consistent with the suggestion by Arnoult et al. (2000) that the  $6.9\ \mu\text{m}$  feature detected in objects such as IRAS 22272+5435 could be caused by the methylene scissoring mode. Additionally, based on Colthup et al. (1990), Arnoult et al. argued that the shape and position of the methylene scissoring feature could be diagnostic of the structure of carbon atoms

adjacent to the methylene group. For example, if a methylene subunit is part of an aliphatic chain, the frequency of the mode ( $\sim 1463\ \text{cm}^{-1}$ ) is slightly higher than if the methylene is adjacent to one or more aromatic subunits ( $\sim 1440\ \text{cm}^{-1}$ ), as is the case in many of our  $\text{H}_n$ -PAHs. This means that the center of the methylene scissoring feature can shift depending on the structure of the molecule and the number of neighboring methylene groups. Specifically, this has the effect of either redshifting the methylene scissoring feature if the molecules are mostly aromatic with few methylene subunits, or blueshifting the methylene scissoring feature in the case when they exist mostly within an aliphatic chain.

In order to test whether the suggestion of Arnoult et al. (2000) applies to these  $\text{H}_n$ -PAHs, we used the co-additions described above, and shown in Figures 3 and 4, to compare the co-added methylene scissoring bands of our minimally hydrogenated, heavily hydrogenated, and fully hydrogenated molecules (see Figure 7). In order to more closely mimic astronomical spectra, which are observed in emission,

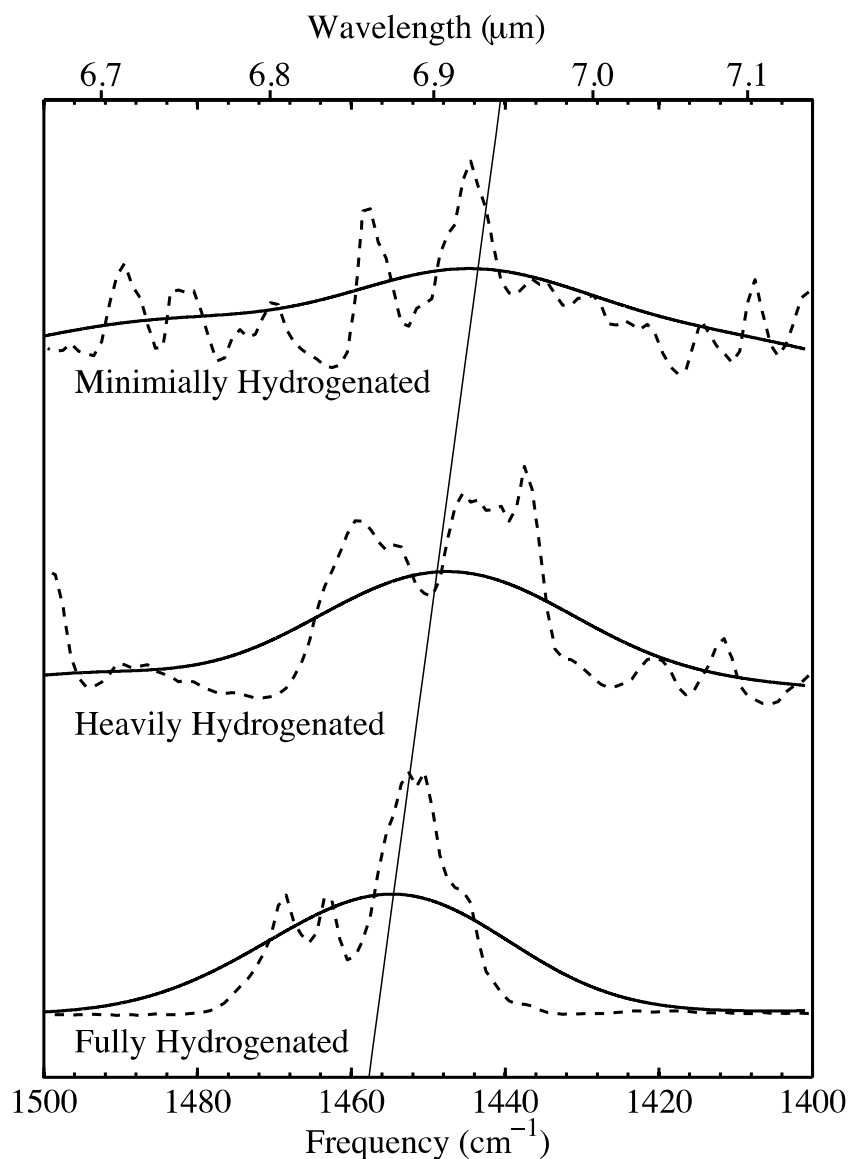


**Figure 7.** Co-added laboratory spectra of minimally, heavily, and fully hydrogenated  $H_n$ -PAHs in the region of the methylene scissoring vibration region (dashed lines) near  $6.9 \mu\text{m}$ . Solid lines show how these co-add features would look in emission assuming a broadening of  $30 \text{ cm}^{-1}$ . The vertical line illustrates the shift of this feature to the blue with increasing hydrogenation.

we have also provided curves that more closely represent the widening of this band expected from  $H_n$ -PAHs in emission. Each point in the laboratory spectra was assigned a Gaussian profile with a  $30 \text{ cm}^{-1}$  FWHM, consistent with the expected natural linewidth for emitting PAH molecules (Allamandola et al. 1985, 1989b). Figure 7 shows that the center of the methylene scissoring band becomes progressively more blueshifted as molecules undergo increasing hydrogenation. This progressive shift correlates with the statistically increasing likelihood of a methylene group having adjacent methylene groups as the ratio of aliphatic to aromatic subunits increases and is entirely consistent with the suggestions of Arnoult et al. (2000).

This spectral behavior can be used to interpret astronomical data in the context of the possible presence of  $H_n$ -PAHs. Figure 8 shows the spectra in the  $6.9 \mu\text{m}$  region of IRAS 21282+5050, IRAS 22272+5435, and IRAS 04296+3429, the same objects for which we earlier discussed the spectra in the C–H stretching region. For IRAS 21282+5050, a normal PAH emitter with

C–H stretch features that suggest the lowest possible relative abundance of  $H_n$ -PAHs, the main feature in the  $6.9 \mu\text{m}$  region is quite broad, so weak that it is barely distinguishable from the baseline, and is actually centered at  $\sim 7 \mu\text{m}$  ( $\sim 1420 \text{ cm}^{-1}$ ) (Figure 8). This position is highly redshifted relative to the normal methylene scissoring position and is thus unlikely related to this chemical moiety. In contrast, the main features in the  $6.9 \mu\text{m}$  region of both IRAS 22272+5435 and IRAS 04296+3429 fall within the expected band position for methylene scissoring (Figure 8). Comparison of the position of the  $6.9 \mu\text{m}$  feature in both IRAS 22272+5435 and IRAS 04296+3429 to the co-added laboratory data suggests that these emission spectra were produced by heavily hydrogenated  $H_n$ -PAH molecules. In summary, *the  $6.9 \mu\text{m}$  data suggest that the emission spectra of both IRAS 22272+5435 and IRAS 04296+3429 are consistent with the presence of significant quantities of  $H_n$ -PAHs, as also implied by their C–H stretching features, while the spectrum of IRAS 22272+5435 is not consistent with any significant contributions from  $H_n$ -PAHs.*

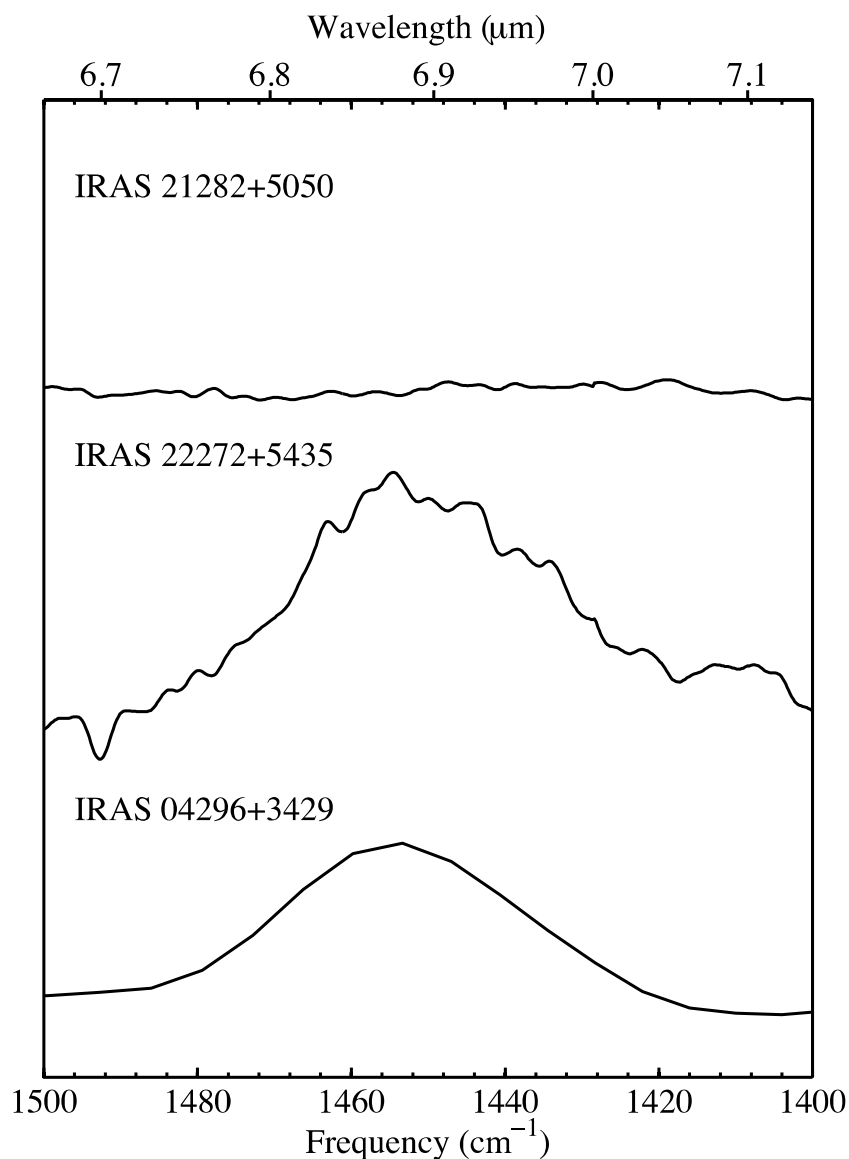


**Figure 8.** The reprocessed 6.7–7.1  $\mu\text{m}$  spectra of IRAS 21282+5050 using ISO SWS 01 as part of the MUIZON.MMDUSTY proposal (observation ID: 15901777, observation date: 1996–04–24T14:44:06), IRAS 22272+5435 using ISO SWS 01 as part of the PROCHE.STARDUST proposal (observation ID: 36601502, observation date: 1996–11–17T02:39:12), and IRAS 04296+3429 using *Spitzer* IRSX 0 IrsStare as part of the Deuterium Enrichment in PAHs program (Request key: 4116736, observation date: 2007–02–05T20:18:27). The strengths of the features have been scaled against each object’s respective 6.2  $\mu\text{m}$  feature (not shown). Underlying continuum spectra have been removed for each object.

## 5. CONCLUSIONS

$H_n$ -PAHs, polycyclic aromatic hydrocarbons having excess H atoms, are potentially important subclass of PAH-related materials in a variety of astrophysical environments. In this paper, we have analyzed and presented a series of mid-infrared spectra (4000–500  $\text{cm}^{-1}$ , 2.5–20  $\mu\text{m}$ ) for 23  $H_n$ -PAHs that span a wide range of excess hydration. These data show a consistent series of varying spectral characteristics that correlate with H addition.

First, as the level of hydrogenation of base PAH structure increases, the aromatic C–H stretch band strength decreases and aliphatic bands rapidly grow in their place. This is plainly seen in molecular families showing progressive levels of hydrogenation (for example, for naphthalene and the various  $H_n$ -naphthalenes in Series A), or by examining co-additions of different sets of molecules that have similar levels of excess hydrogenation. Because the aliphatic C–H stretch has a stronger intrinsic strength,

and there are more H atoms per carbon for aliphatic groups, the aliphatic bands begin to dominate over aromatic bands in the C–H stretching region even for molecules with only moderate excess H coverage. The level of hydrogenation can be approximately determined from the relative strengths of the aromatic and aliphatic C–H stretch bands. By their very nature, the aliphatic C–H stretches in  $H_n$ -PAHs are completely dominated by the  $-\text{CH}_2-$  asymmetric and symmetric stretching modes near 2940 and 2860  $\text{cm}^{-1}$  (3.40 and 3.50  $\mu\text{m}$ ), respectively; they produce no significant absorption at the positions of the  $-\text{CH}_3$  asymmetric and symmetric stretching modes.

Second, the position of the aliphatic C–H stretching bands is affected by strain when adjacent to neighboring aromatic or olefinic moieties. This strain causes blueshifting of the associated aliphatic C–H stretching modes relative to the canonical position of this mode in fully aliphatic molecules. This strain is completely removed when the molecule is fully hydrogenated (at which point it is essentially a polycyclic aliphatic

hydrocarbon) and the C–H stretching features fall at the same positions as seen for –CH<sub>2</sub>– groups in fully aliphatic, linear compounds.

Third, hydrogenation of PAHs also produces a feature near 6.9  $\mu\text{m}$  (1450  $\text{cm}^{-1}$ ) due to methylene scissoring motions of the new –CH<sub>2</sub>– groups within the rings. As hydrogenation increases, the methylene scissoring band grows. Like the aliphatic C–H stretching mode bands, the position of the methylene scissoring mode shifts in response to strains caused by adjacent aromatic or olefinic moieties, but in this case the result is a shift to the red instead of the blue. As with the C–H stretching bands, full hydrogenation removes these strains and results in a band whose position is very similar to that of saturated aliphatic, linear molecules.

Finally, C–H out-of-plane bending mode bands, which dominate PAH spectra in the 10–15  $\mu\text{m}$  (1000–670  $\text{cm}^{-1}$ ) region are radically changed or eliminated by hydrogenation. The details of these changes depend on molecular structure, the degree of hydrogenation, and the molecular locations of the excess H atoms.

These laboratory data have important potential implications for the interpretation of objects that show PAH emission features, particularly those that show anomalously strong emission at 3.4  $\mu\text{m}$ . The aliphatic C–H stretch in H<sub>n</sub>-PAHs has been suggested as a potential explanation for some of the 3.4  $\mu\text{m}$  band seen in emission in PAH-containing objects, particularly in those objects that show anomalously large 3.4  $\mu\text{m}$  features (Bernstein et al. 1996). Our laboratory results are fully consistent with this explanation. However, we should note that, even in those objects with very large 3.4  $\mu\text{m}$ /3.3  $\mu\text{m}$  band area ratios, the absolute degree of implied excess hydrogenation is not large. Even in objects with very large 3.4  $\mu\text{m}$ /3.3  $\mu\text{m}$  ratios, the molecular population is still dominated by aromatic carbon, not aliphatic carbon.

We compared our new laboratory data with emission spectra from IRAS 21282+5050, an object with normal PAH emission features and from IRAS 22272+5435 and IRAS 04296+3429, two protoplanetary nebulae with abnormally large 3.4  $\mu\text{m}$  features. Assuming H<sub>n</sub>-PAHs are responsible for the 3.4  $\mu\text{m}$  feature, and using laboratory data as a reference, limits on the ratio of  $N_{\text{aliphatic H}}$  to  $N_{\text{aromatic H}}$  are shown to be 0.16, 0.47, and 0.65 for IRAS 21282+5050, IRAS 22272+5435, and IRAS 04296+3429, respectively. The position of the 3.4  $\mu\text{m}$  feature in each of the astronomical objects is slightly blueshifted relative to the canonical position of the methylene asymmetric stretch, consistent with residence in hydrogenated rings strained by neighboring aromatic or olefinic moieties. IRAS 22272+5435 and IRAS 04296+3429 both possess 6.9  $\mu\text{m}$  features whose position and relative strength are consistent with the presence of H<sub>n</sub>-PAH molecules, however, IRAS 21282+5050 does not. These results suggested that partially hydrogenated H<sub>n</sub>-PAHs may represent a significant component of the organic inventory in proto-planetary nebulae such as IRAS 22272+5435 and IRAS 04296+3429, while IRAS 21282+5050, a normal PAH emitter, does not appear to have a significant inventory of H<sub>n</sub>-PAHs based on the lack of a significant 6.9  $\mu\text{m}$  emission feature in its spectrum. This suggests that the features in the 3.4  $\mu\text{m}$  region of IRAS 21282+5050, and by extension, in other “normal” PAH emission objects, are likely to be largely due to other sources like overtones and combinations of lower frequency PAH vibrational modes and “hot” bands associated with relaxation of higher anharmonic vibrational modes of the aromatic C–H stretch.

This work demonstrates that H<sub>n</sub>-PAHs should be added to the mix of PAH-related molecules (PAH neutrals and ions, PAHs with heteroatoms, etc.) that are used to fit astronomical spectra that show the family of infrared emission features typically associated with PAHs. They are likely to be particularly important for explaining the spectra of objects in which H<sub>n</sub>-PAHs may be expected. Such environments include protoplanetary nebulae where less harsh radiation fields have yet to winnow out less stable molecular species in the outflows of dying stars and in locations where H II regions are eating into adjacent dense cloud materials and liberating PAHs that may have been irradiated while trapped in ices.

The authors would like to thank C. Bauschlicher, L. Allamandola, A. Mattioda, and an anonymous reviewer for helpful comments and suggestions provided during the very long duration of this work. We would like to thank D. Hudgins for providing the previously unpublished spectrum of benzo[a]pyrene. We are also grateful to J. Dworkin for doing HPLC work to establish the purity of several of our compounds. The paper also benefited greatly from excellent technical support by R. Walker. We are also grateful to M. Vala and J. Szczepanski for kindly providing us with their spectral data for fluorine (Szczepanski et al. 2002) which appears in the Appendix. Finally, the authors are grateful for funding from NASA grants from the Origins of Solar Systems, Exobiology, Astrobiology, and Astrophysics Programs, which made this work possible.

## APPENDIX

### A.1. Series B (Anthracene, DHA, HHA)

The 3200–2700 and 2000–500  $\text{cm}^{-1}$  spectra of matrix isolated anthracene and H<sub>n</sub>-anthracenes are presented in Figures 9 and 10, respectively. The positions and relative strengths of absorption bands are listed in Tables 7 and 8.

Anthracene possesses only aromatic C–H stretching modes that span a narrow range of frequencies around 3065  $\text{cm}^{-1}$  (Hudgins & Sandford 1998a). In dihydroanthracene (DHA; an H<sub>2</sub>-anthracene), the hydrogen atoms were added to the central ring, destroying its aromaticity. The aromatic C–H bands in DHA span 3126–2998  $\text{cm}^{-1}$ . The main features of the aliphatic bands in DHA are located from 2993 to 2773  $\text{cm}^{-1}$ . In the isomer of hexahydroanthracene (HHA; H<sub>6</sub>-anthracene) measured for this paper, hydrogen atoms were added to all of the rings, the aromaticity has been lost, along with the bands associated with the aromatic C–H stretch, but C–H stretches associated with olefinic hydrogens have grown in their place around 3040  $\text{cm}^{-1}$ . The majority of the aliphatic C–H stretch bands in HHA appear between 2912 and 2796  $\text{cm}^{-1}$  with a small feature between 3006 and 2973  $\text{cm}^{-1}$ .

At lower frequencies, a skeletal deformation mode may account for the bands at 603 and 608.8  $\text{cm}^{-1}$  in anthracene and DHA, respectively. Anthracene possesses strong bands around 728 and 878  $\text{cm}^{-1}$  associated with the quartet and solo aromatic C–H<sub>OOP</sub> bending respectively (Hudgins & Sandford 1998a). In DHA, the solo C–H<sub>OOP</sub> bend disappears, as expected, and bands appear at 762.3, 746.5, and 730.7  $\text{cm}^{-1}$ . In HHA, there are no aromatic out-of-plane bends, but there is a band that falls in the typical range for olefinic C–H<sub>OOP</sub> bending modes around at 655.6  $\text{cm}^{-1}$ . As seen in the naphthalene series, anthracene possesses bands from 1600 to 1000  $\text{cm}^{-1}$  that may be attributed to the C–H in-plane bending, aromatic carbon

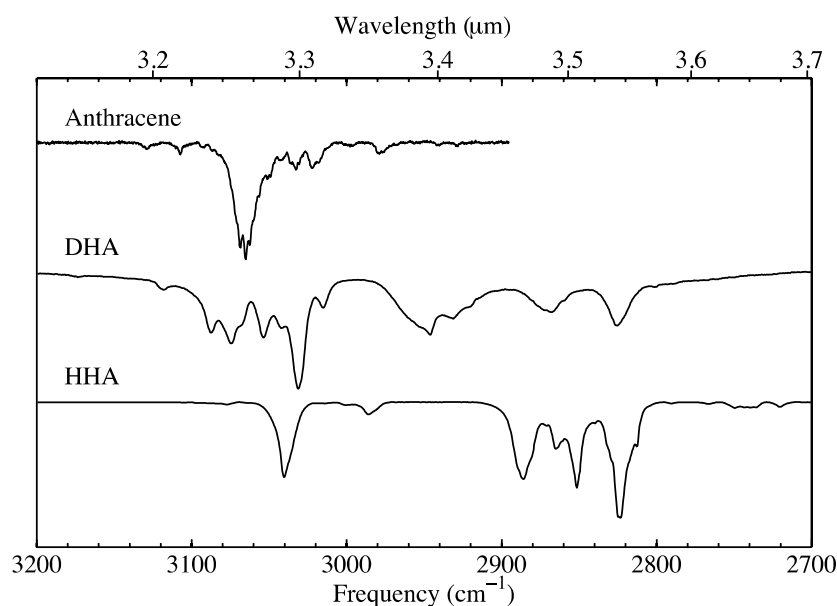


**Figure 9.** The 3200–2700  $\text{cm}^{-1}$  CH stretch region spectra of molecules in Series B (anthracene skeletal structure). The spectrum of anthracene is from Hudgins & Sandford (1998a).

**Table 7**  
9,10-dihydroanthracene (DHA)

Band Position ( $\text{cm}^{-1}$ )	Normalized Band Area
608.8	0.31
730.7	<b>1.00</b>
746.5	0.37
762.3	0.60
959.6, 954.6*	0.12
1040.5	0.08
1122.1	0.07
1158.5, 1151.5*	0.05
1183.9	0.05
1208.2	0.12
(1436–1419): 1431.0, 1427.7*, 1425.0	0.20
(1516–1444): 1506.0, 1500.1, 1496.2, 1490.5, 1487.7*, 1480.0*, 1469.5, 1466.7, 1456.7*	1.54
1581.8*, 1576(sh)	0.07
1608.0*, 1600.5	0.05 <sup>a</sup>
1797.8	0.06
1945.0	0.05
(2993–2773): 2945.3*, 2930.6, 2867.1*, 2824.4*	1.76
(3126–2998): 3117.4, 3086.4, 3073.5, 3066(sh), 3052.8, 3041.0, 3030.1*, 3014.2	1.72

**Note.** <sup>a</sup>An approximate 5% contribution from absorption by contaminant  $\text{H}_2\text{O}$  has been removed.

skeletal stretching, and overtone/combination modes. Once again, bands associated with methylene scissoring grow in the 1513–1430  $\text{cm}^{-1}$  region as the molecule becomes progressively more hydrogenated.

**Table 8**  
1,4,5,8,9,10-hexahydroanthracene (HHA)

Band Position ( $\text{cm}^{-1}$ )	Normalized Band Area
655.6	<b>1.00</b>
846.7	0.13
987.5*, 983.3*, 978.7	0.62
1249.8, 1247.2	0.05
1350.9, 1344.7*	0.05
(1443–1420): 1436.8*, 1428.4, 1423.8	0.44
1665.2	0.07 <sup>a</sup>
2692.9, 2675.3*	0.10
(2759–2728): 2748.6, 2742.2, 2738.5, 2735.1	0.13
(2912–2796): 2885.1*, 2870.2, 2863.6, 2850.5*, 2838.6, 2822.9*, 2811.8	5.73
(3006–2973): 3000.1, 2984.9*	0.18
(3059–3021): 3039.4	1.22
(3093–3069): 3076.4	0.03

**Note.** <sup>a</sup>An approximate 15% contribution from absorption by contaminant  $\text{H}_2\text{O}$  has been removed.

#### A.2. Series C (Phenanthrene, DHPH, DBS, Fluorene, t-PHF)

The 3200–2700 and 2000–500  $\text{cm}^{-1}$  spectra of matrix isolated phenanthrene and  $\text{H}_n$ -PAHs with a phenanthrene-like skeletal structure are presented in Figures 11 and 12, respectively. The positions and relative strengths of absorption bands are listed in Tables 9–11.

Phenanthrene's aromatic C–H stretch bands range from 3140 to 3000  $\text{cm}^{-1}$  (Hudgins & Sandford 1998a). The aromatic C–H stretch bands of DHPH span the region of 3099–3012  $\text{cm}^{-1}$ . DBS, which has a seven-member central ring, has a similar profile to DHPH, but there is some intensity shifted to the lower

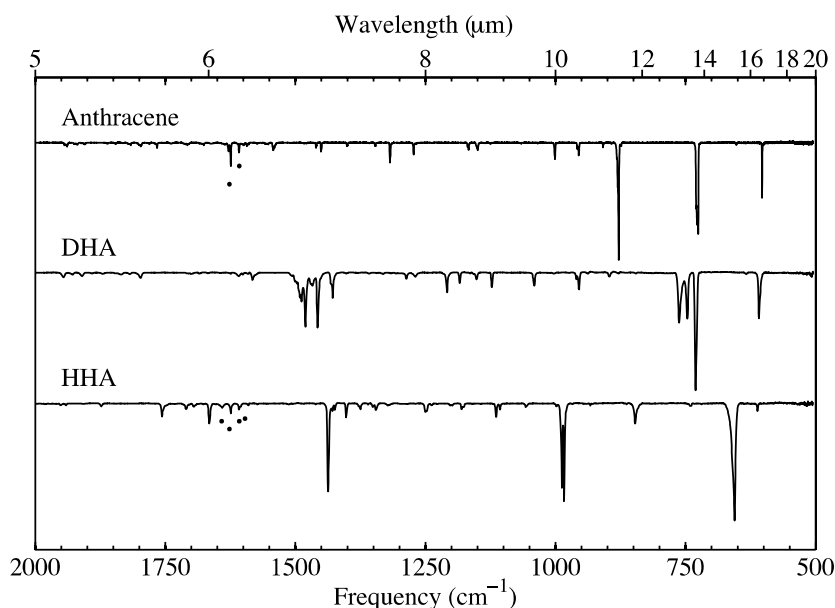


**Figure 10.** The 2000–500  $\text{cm}^{-1}$  transmission spectra of molecules in Series B (anthracene skeletal structure). The spectrum of anthracene is from Hudgins & Sandford (1998a). A (\*) denotes bands due to trace  $\text{H}_2\text{O}$  contamination.

**Table 9**  
9,10-dihydrophenanthrene (DHPH)

Band Position ( $\text{cm}^{-1}$ )	Normalized Band Area
622.3*, 619.4(sh)	0.08
(733–723): 731.0(sh), 728.0, 726.3*	0.11
746.4	<b>1.00</b>
(783–768): 779.7, 777.1 774.2*, 772.4*, 769.2	0.15
1447.5*, 1442.3	0.16
1458.1	0.18
(1493–1482): 1491.0(sh), 1489.3*, 1485(sh)	0.21
2847.0	0.14
(2981–2891): 2968(sh), 2949.7*, 2936(sh), 2920.4, 2907.3, 2901	0.63
(3056–3012): 3046.5*, 3037.7, 3030.3, 3024.0, 3016.7	0.22
(3099–3057): 3079.3*, 3063.1	0.24

end of the frequency range for the aromatic C–H stretches. The spectrum of fluorene, which possesses a five-member central ring, shows a series of aromatic bands from 3114 to 3002  $\text{cm}^{-1}$  (Szczepanski et al. 2002). In DHPH, which has four additional hydrogens, several bands appear in the C–H aliphatic stretching region between 2981 and 2891 and around 2847  $\text{cm}^{-1}$ . In DBS, which has six aliphatic hydrogens, the aliphatic stretch region has become considerably more crowded with many overlapping bands from 2994 to 2825  $\text{cm}^{-1}$ . Fluorene, with its two aliphatic hydrogens, shows a dense cluster of bands from 2953 to 2887  $\text{cm}^{-1}$ , in addition to a single band at 2803.2  $\text{cm}^{-1}$ . The aliphatic C–H stretch in *t*-PHF possesses overlapping bands spanning the region between 3002 and 2836  $\text{cm}^{-1}$ .

At longer wavelengths, a low frequency mode that may be associated with skeletal deformations appears around 620  $\text{cm}^{-1}$

**Table 10**  
Dibenzosuberane (DBS)

Band Position ( $\text{cm}^{-1}$ )	Normalized Band Area
585.7	0.15
625.0	0.23
700.5	0.05
710.3	0.09
738.4*, 735.5	0.59
749.4*, 747(sh)	0.83
762.0	<b>1.00</b>
913.7*, 910.2	0.05
949.5	0.06
(1111–1090): 1105.9, 1103.2*, *1097.4, 1091.8	0.20
1231.8, 1225.3*	0.07
(1317–1284): 1313.5, 1311.0, 1307.6, 1300.0*, 1293.2*, 1288.1	0.17
1364(sh), 1361.3*	0.14
1436.8*, 1429.7	0.14
(1473–1443): 1466.2, 1460.3*, 1449.8*	0.59
1498.2*, 1489.9	0.90
1946.2, 1943.7	0.05
(2994–2825): 2981.4, 2941.2*, 2921.7, 2910.9, 2897.9, 2882.1, 2868.9, 2865.6, 2862.2, 2847.4	1.95
(3134–2996): 3113.8, 3083(sh), 3073.6*, 3066.0, 3056.9, 3053(sh), 3031.2*, 3023.5, 3005(sh)	1.37

in phenanthrene (Hudgins & Sandford 1998a). The same feature appears in the remaining molecules with intact aromatic rings in this series but is missing in the fully aliphatic perhydrofluorene. In phenanthrene, quartet and duet C–H<sub>OP</sub> bands appear around

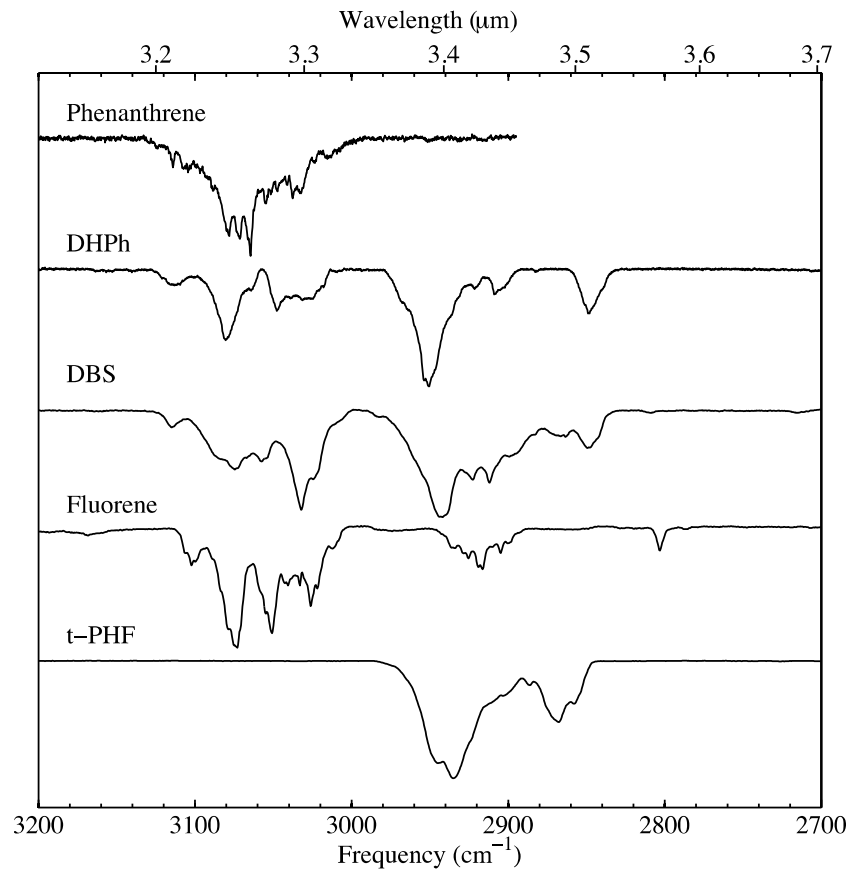


**Figure 11.** The 3200–2700  $\text{cm}^{-1}$  CH stretch region spectra of molecules in Series C. The spectrum of phenanthrene is taken from Hudgins & Sandford (1998a) and the spectrum of fluorene is taken from Szczepanski et al. (2002).

**Table 11**  
*trans*-perhydrofluorene (*t*-PHF)

Band Position ( $\text{cm}^{-1}$ )	Normalized Band Area
853.1	0.07
1371.9, 1366.8*, 1361.5	0.09
(1480–1438): 1466.8*, 1458.0, 1452.9*, 1446.6	<b>1.00</b>
(2718–2612): 2697.3, 2670.9*, 2642(sh)	0.38
(3002–2836): 2944.9, 2933.6*, 2900(sh), 2885.9, 2868.1*, 2857(sh)	24.24

**Table 12**  
4,5-dihydropyrene (DHP)

Band Position ( $\text{cm}^{-1}$ )	Normalized Band Area
705.3, 698.8	0.05
725.2	0.53
755.4	0.26
830.9, 827(sh)	<b>1.00</b>
853.3	0.06
1089.8	0.05
1167.1*, 1161.9	0.05
1187.0(sh), 1183.9*	0.06
(1247–1229): 1244.2, 1237.3*, 1232.2	0.06
(1317–1299): 1313.6, 1308.5*, 1302(sh)	0.11
(1462–1411): 1447.4*, 1442.1, 1436.1, 1426.1, 1417.2	0.46
1790.3*, 1785.1	0.05
(2985–2811): 2956.0, 2942.1*, 2896.5, 2885(sh), 2861.4, 2837.6	1.20
(3131–2988): 3120.4, 3096.8, 3057.5*, 3029.0, 3019.0	1.09

735.3 and 813  $\text{cm}^{-1}$ , respectively. In DHPPh, the duet bands from phenanthrene disappear leaving only quartet bands around 746.4 with  $\text{cm}^{-1}$  small features appearing around 772 and 728  $\text{cm}^{-1}$ . In DBS three large C–H<sub>OOP</sub> features appear around 738, 748, and 762  $\text{cm}^{-1}$ . In the spectrum of fluorene, the C–H<sub>OOP</sub> bending band appears near 740  $\text{cm}^{-1}$  (Szczepanski et al. 2002). All but the final member of this series possesses bands associated with the C–H in-plane bending, and aromatic carbon skeletal stretching. Bands associated with methylene scissoring appear between 1510 and 1420  $\text{cm}^{-1}$  in all members of the series excluding phenanthrene. In *t*-PHF, these scissoring modes are the largest features in this region of the spectrum.

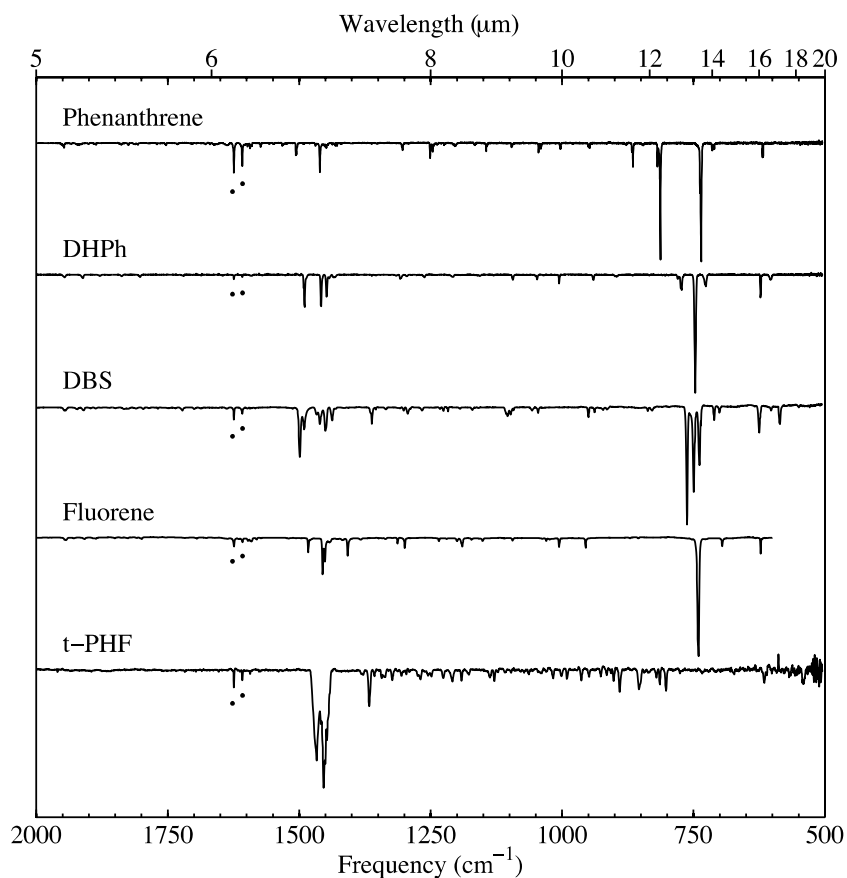


**Figure 12.** The 2000–500  $\text{cm}^{-1}$  spectra of molecules in Series C. The spectrum of phenanthrene is taken from Hudgins & Sandford (1998a) and the spectrum of fluorene is taken from Szczepanski et al. (2002). A (\*) denotes bands due to trace  $\text{H}_2\text{O}$  contamination.

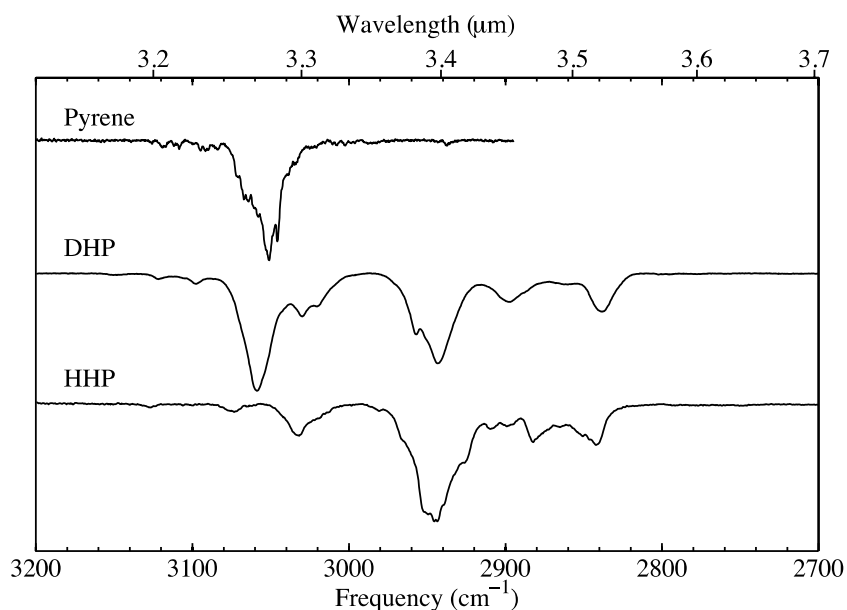


**Figure 13.** The 3200–2700  $\text{cm}^{-1}$  CH stretch region spectra of molecules in Series D (pyrene skeletal structure). The spectrum of phenanthrene is taken from Hudgins & Sandford (1998a).

### A.3. Series D (Pyrene, DHP, HHP)

The 3200–2700 and 2000–500  $\text{cm}^{-1}$  spectra of matrix isolated pyrene and  $\text{H}_n$ -PAHs with a pyrene skeletal structure are presented in Figures 13 and 14, respectively. The positions and relative strengths of absorption bands are listed in Tables 12

and 13. The C–H stretching region of HHP has previously been examined in Bernstein et al. (1996).

Pyrene possesses aromatic C–H stretch bands centered ranging from 3080 to 3020  $\text{cm}^{-1}$  (Hudgins & Sandford 1998a). In DHP, the C–H aromatic stretch bands are no longer clustered into one main feature and now appear as two overlapping

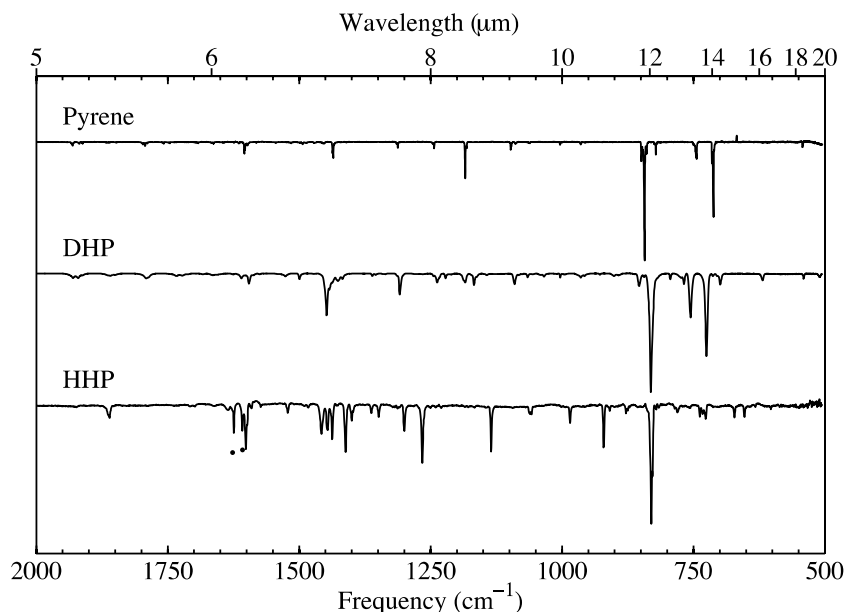


**Figure 14.** The 2000–500  $\text{cm}^{-1}$  spectra of molecules in Series D (pyrene skeletal structure). The spectrum of phenanthrene is taken from Hudgins & Sandford (1998a). A (\*) denotes bands due to trace  $\text{H}_2\text{O}$  contamination.

**Table 13**  
1,2,3,6,7,8-hexahydropyrene (HHP)

Band Position ( $\text{cm}^{-1}$ )	Normalized Band Area
652.8	0.05
737.5, 732.7, 726.4	0.17
785.4, 780.4*	0.07
(841–824): 838(sh), 829.9*, 827.6	<b>1.00</b>
(884–866): 878.2*, 875.4, 871.6	0.10
920.5	0.18
984.4	0.07
1061.9, 1060.4	0.07
1134.7	0.20
1265.3	0.38
1299.8	0.15
1353.9, 1348.5*	0.07
1399.7*, 1396.9	0.10
1411.2*, 1407(sh)	0.28
(1467–1431): 1457.4, 1446.9, 1445.5, 1436.9	0.66
1521.3	0.06
1601.0*, 1598.4	0.29 <sup>a</sup>
1863.0(sh), 1860.1*	0.11
(2991–2817): 2979.3, 2965(sh), 2949.6, 2943.2*, 2925.1(sh), 2907.9, 2897.1, 2881.5, 2864.4, 2849.8, 2840.8	9.41
(3055–3000): 3031.5*, 3017(sh)	1.02
3073.1	0.14

**Note.** <sup>a</sup>A contribution from absorption by contaminant  $\text{H}_2\text{O}$  has been removed.

**Table 14**  
Benzo[a]pyrene

Band Position ( $\text{cm}^{-1}$ )	Normalized Band Area
534.7	0.10
636.2*, 637.4	0.10
691.6	0.34
711.8*, 712.6, 715.0	0.11
741.7*, 743.7	0.39
751.5	0.08
<b>761*, 763.0, 766.0</b>	1.00
814.1	0.14
827.3*, 828.7, 830.7	0.30
839.4	0.11
842.7, 834.7, 845.6	0.15
849.3, 851.0*	0.28
881.5*, 882.3*	0.44
1024.1	0.05
1038.7	0.04
1182.2*, 1183.8, 1180.9	0.17
1194.9, 1200.7*	0.05
1243.1, 1246.0	0.05
1264.3, 1271.8, 1273.3	0.08
1312.1, 1315.4	0.07
1411.3, 1417.2, 1419.8	0.12
(1521.3–1448): 1460.1, 1467.4, 1479.4, 1498.4, 1516.0	0.44
1755.5, 1762.0	0.07
1779.3, 1793.0	0.07
(1951–1887): 1889.7, 1915.0, 1919.2, 1930.5, 1942.4	0.18
(3139.5–2964): 2982.0, 3045*, 3060.7, 3088.2, 3105.1	1.08

**Table 15**  
7,8,9,10-tetrahydrobenzo[a]pyrene (THB[a]P)

Band Position ( $\text{cm}^{-1}$ )	Normalized Band Area
516.6	0.09
535.4	0.05
682.8	0.08
713.5	0.86
757(sh), 753.9*	0.29
804.6	0.22
816.8	<b>1.00</b>
825.2	0.13
834.2	0.22
843.9	0.49
874.5	0.64
881.7	0.07
909.6	0.09
1078.9	0.07
1188.6, 1181.8*	0.32
1253.4	0.28
1265.2	0.12
1273.4	0.05
1303.5, 1300.4	0.15
1360.1	0.10
1420.9*, 1418.5	0.15
1445.7, 1440.6	0.46
1452.5	0.05
1463.6	0.07
1486.3	0.11
1590.4	0.19
1605.4	0.31
(2984–2806): 2947.7*, 2922(sh), 2892.4, 2872.5, 2845.3	10.06
(3094–2991): 3061.4	2.82

features from 3085 to 2988  $\text{cm}^{-1}$ , and two small features from 3110 to 3090 and 3131 to 3115  $\text{cm}^{-1}$ , respectively. In HHP, there are one large and two small aromatic C–H stretch features from 3055 to 3000, 3090 to 3058, and 3138 to 3120  $\text{cm}^{-1}$ , respectively. The aliphatic stretch profiles are similar in DHP and HHP, both showing  $-\text{CH}_2-$  features approximately spanning the range of 2990–2810  $\text{cm}^{-1}$ .

At lower frequencies, the spectrum of pyrene, shows large, trio C–H<sub>oop</sub> bands at 712.0 and 745.0  $\text{cm}^{-1}$  with a duet band at 843.0  $\text{cm}^{-1}$  (Hudgins & Sandford 1998a). DHP possesses a more complicated series of C–H<sub>oop</sub> bands with a trio features at 725.2 and 755.4 and a large duet feature at 830.9  $\text{cm}^{-1}$ . HHP possesses no trio hydrogens, and as a result, only the duet feature is observed around 830  $\text{cm}^{-1}$ . All members of this series possess bands associated with the C–H in-plane bending, and aromatic carbon skeletal stretching, as well as overtones and combination modes. Bands associated with methylene scissoring appear between 1462 and 1411  $\text{cm}^{-1}$  in DHP, and between 1467 and 1390  $\text{cm}^{-1}$  in HHP.

**Table 16**  
9H-cyclopenta[a]pyrene (9H-Cp[a]P)

Band Position ( $\text{cm}^{-1}$ )	Normalized Band Area
645.6, *642.7	0.05
681.1, *674.7	0.06
704.8	<b>1.00</b>
*755.5, 753.2	0.18
798.8	0.17
820.6	0.43
*842.7, 837.7	0.34
(883–866): 881.1, 874.4*, 868.8	0.55
917.7	0.17
(954–938): 949.1, *943.5, 942	0.23
1145.5	0.05
(1190–1170): 1186.9, *1180.3, 1172.9	0.16
1270.5	0.07
1351.7, *1344.9	0.11
1400.2	0.18
1420.7	0.08
(1441–1428): *1435.8, *1433.8, 1429.5	0.23
*1599.4, 1594.4	0.15
(1869–1849): 1864.0, *1859.5, 1856.0, 1851.3	0.05
(1938–1906): *1928.9, 1924.3, *1920.1, 1917.8, *1913.5	0.11
(2799–2762): 2793.2, *2776.8, 2768.2	0.05
(2996–2838): 2963.4, 2931.7*, 2915.6, 2902.1*, 2893.5, 2860.6*	1.34
(3149–2997): 3099.1, 3077.7, 3060(sh), 3044.8*, 3026.4, 3011.8	1.61

#### A.4. Series E (Benzo[a]pyrene, THB[a]P, 9H-Cp[a]P, HHCp[a]P)

The 3200–2700 and 2000–500  $\text{cm}^{-1}$  spectra of matrix isolated benzo[a]pyrene, an  $\text{H}_n$ -PAH with a benzo[a]pyrene skeleton, and members of the cyclopenta[a]pyrene family are presented in Figures 15 and 16, respectively. The positions and relative strengths of absorption bands associated with the spectra of these molecules are listed in Tables 14–17.

The benzo[a]pyrenes possess very similar aromatic C–H stretch bands from 3100 to 2990  $\text{cm}^{-1}$ . The aliphatic bands appear between 2984 and 2806  $\text{cm}^{-1}$  in THB[a]P.

Changing the six-member ring added on to pyrene to a five-member ring makes it impossible to have a totally aromatic molecule, and as a result 9H-Cp[a]P is the least hydrogenated variant of this structure. The spectrum of 9H-Cp[a]P shows a series of broad aromatic C–H stretch bands from 3149 to 2997  $\text{cm}^{-1}$ , in addition to small aliphatic bands between 2996 and 2838  $\text{cm}^{-1}$  and between 2800 and 2755  $\text{cm}^{-1}$ . In HHCp[a]P, aromatic bands fall between 3100 and 3000  $\text{cm}^{-1}$  and aliphatic bands fall between 2992 and 2819  $\text{cm}^{-1}$ .

**Table 17**

4,5,7,8,10,11-hexahydro-9H-cyclopenta[a]pyrene (HHCp[a]P)

Band Position (cm <sup>-1</sup> )	Normalized Band Area
636.1	0.11
649.9	0.06
723.6	0.10
750.0*, 743.8*, 738.6	0.61
773.6	<b>1.00</b>
793.2	0.20
866.1*, 883.5	1.42
1008.2, 1005.1	0.05
1042.3, 1037.1	0.12
1066.9	0.10
1133.1, 1127.3	0.05
1167.9, 1162.7*	0.13
1185.7	0.20
1205.9, 1202.8, 1198.3	0.05
1218.3*, 1212.8	0.24
1242.4	0.20
1262.8	0.06
1281.4*	0.11
(1350–1293): 1344.6, 1328.0, 1334.5, 1319.9, 1311.0*, 1302.1	0.52
1420.5	0.16
(1486–1426): 1479.4, 1465(sh) 1457.0*, 1443.4*, 1435.5, 1431(sh)	4.15
1572.7	0.07
1616.5*, 1614.7	0.05
1789.7, 1786.4	0.05
1853.1	0.06
1928.4, 1921.0, 1918.2*	0.14
(2996–2834): 2952.8*, 2943.2*, 2916.7, 2901.1, 2874.2, 2859.7, 2846.3	25.53
3013.9	0.72
3041.1	0.14
3082.9, 3064.5*	0.24

At longer wavelengths, the members of this series produce very complicated C–H<sub>OOP</sub> bending regions across the 900–650 cm<sup>-1</sup> range and no attempt will be made here to make specific band assignments. Benzo[a]pyrene features bands associated with a quartet (770–735 cm<sup>-1</sup>), a trio (810–750 cm<sup>-1</sup>), two duets (860–800 cm<sup>-1</sup>), and solo (900–860 cm<sup>-1</sup>) aromatic hydrogens. THB[a]P possesses one trio, two duets, and single solo aromatic hydrogen-containing rings. Replacement of the six-member ring in 9H-Cp[a]P with a five-member ring eliminates the quartet bands but introduces olefinic (730–665 cm<sup>-1</sup>) C–H<sub>OOP</sub> bands in addition to the trio, two duet, and solo C–H<sub>OOP</sub> bands from the pyrene. Finally, in HHCp[a]P, the duet and olefinic C–H<sub>OOP</sub> bands are lost. Methylene scissoring modes are found in each spectrum of this series except for benzo[a]pyrene.

**Table 18**

Dodecahydrotriphenylene (DDHTP)

Band Position (cm <sup>-1</sup> )	Normalized Band Area
827.9	0.05
944.9	0.05
1255.7*, 1249.2	0.24
1281.6*, 1275.8	0.07
1315.7	0.21
(1469–1424): 1462.9, 1453.3, 1438.2*	<b>1.00</b>
1582.7	0.07
2679.8	0.11
(2975–2775): 2948.3*, 2941.7, 2924.0(sh), 2878.3, 2871.2, 2861.5, 2838.2, 2807.0	14.49

**Table 19**

Perhydrocoronene (PHC)

Band Position (cm <sup>-1</sup> )	Normalized Band Area
822.8	0.11
990.2	0.19
1021.0	0.05
1047.0	0.20
1170.7	0.09
1213.0	0.15
1296.0, 1292.0*	0.08
1367.0(sh), 1364.1*	0.11
(1463–1434): 1455.3*, 1450.8*, 1445(sh)	<b>1.00</b>
(2956–2710): 2924.9, 2912.2*, 2852.7*, 2821.0(sh)	38.56
2972.3	0.40

#### A.5. Series F (Triphenylene, DDHTP, Coronene, PHC)

The 3200–2700 and 2000–500 cm<sup>-1</sup> spectra of several highly symmetric PAHs and an associated H<sub>n</sub>-PAH variant are presented in Figures 17 and 18, respectively. The positions and relative strengths of absorption bands associated with the spectra of these molecules are listed in Tables 18 and 19. The C–H stretching region of PHC has previously been examined in Bernstein et al. (1996).

The PAHs triphenylene and coronene both possess broad aromatic C–H stretch features from approximately 3150–3020 and 3120–3010 cm<sup>-1</sup>, respectively (Hudgins & Sandford 1998a, 1998b). As expected, their H<sub>n</sub>-PAH variants DDHTP and PHC, show no aromatic C–H stretch character, but instead show broad C–H aliphatic stretches from 2975 to 2775 and 2956 to 2710 cm<sup>-1</sup>, respectively.

The longer wavelength spectra of both triphenylene and coronene are remarkably simple as a result of their high degrees of symmetry (Hudgins & Sandford 1998a, 1998b). This symmetry is broken in the H<sub>n</sub>-PAH versions of these

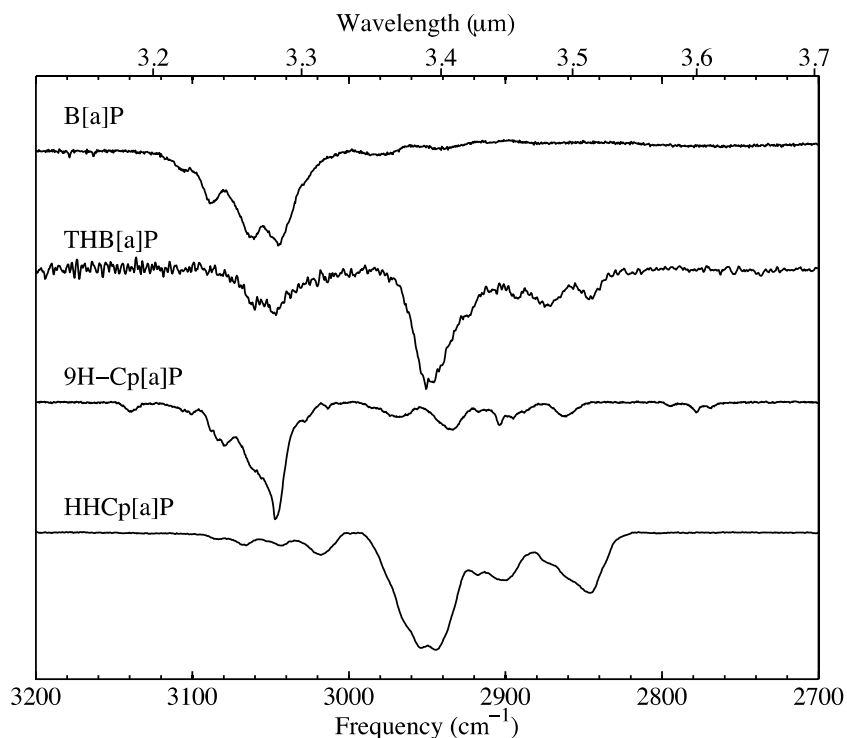


**Figure 15.** The 3200–2700  $\text{cm}^{-1}$  CH stretch region spectra of molecules in Series E (five-ring structures). The spectrum of benzo(a)pyrene is kindly provided by Dr. Doug Hudgins (previously unpublished data).

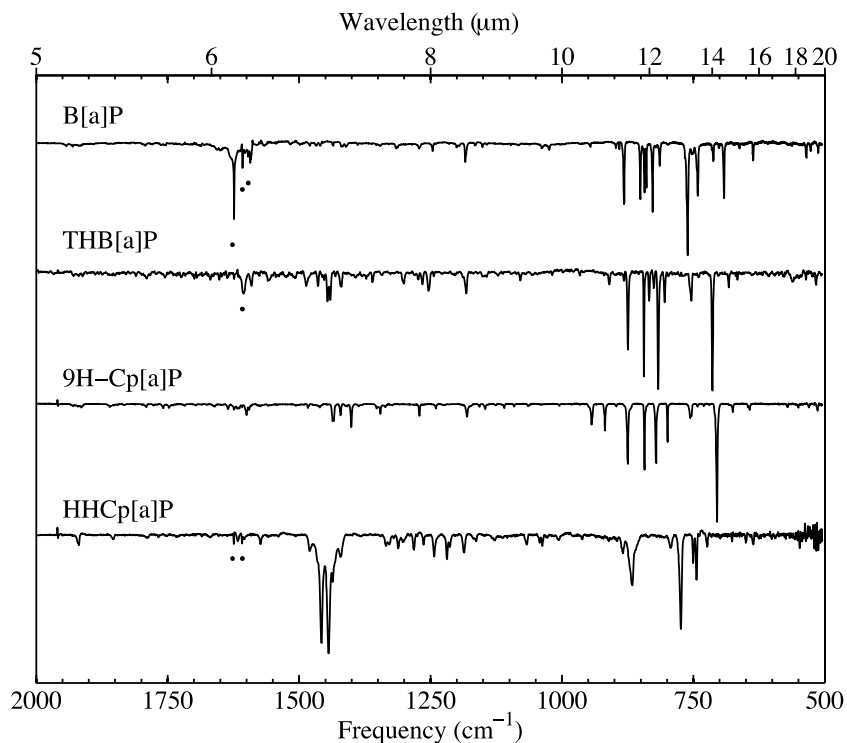


**Figure 16.** The 2000–500  $\text{cm}^{-1}$  spectra of molecules in Series E (five-ring structures). A (\*) denotes bands due to trace  $\text{H}_2\text{O}$  contamination. The spectrum of benzo(a)pyrene is kindly provided by Dr. Doug Hudgins (previously unpublished data).

molecules, however. Triphenylene possesses a strong narrow quartet  $\text{C-H}_{\text{OOP}}$  bend around  $741 \text{ cm}^{-1}$ . There are several small bands associated with  $\text{C-H}$  in-plane bending, and aromatic carbon skeletal stretching, the most prominent of which appear

around at  $1438$  and  $1439 \text{ cm}^{-1}$ . DDHTP has a significantly more complicated spectrum. There are no aromatic hydrogens in DDHTP, and as a result, there is no  $\text{C-H}_{\text{OOP}}$  bend. The most prominent features in DDHTP are strong  $\text{C-H}$  wagging

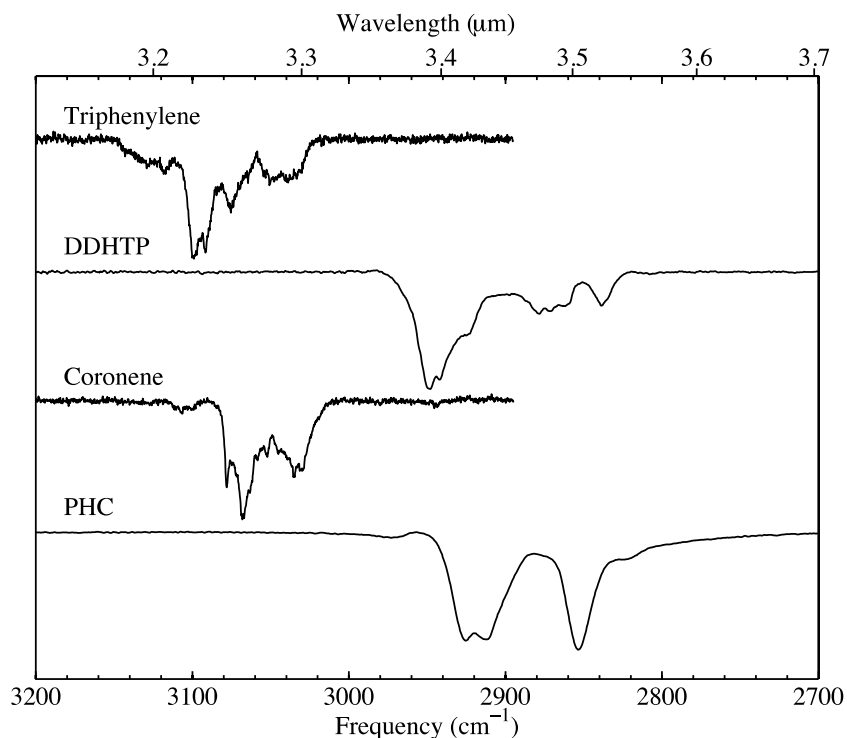


**Figure 17.** The 3200–2700  $\text{cm}^{-1}$  CH stretch region transmission spectra of molecules in Series F. The spectrum of triphenylene is taken from Hudgins & Sandford (1998a) and coronene is taken from Hudgins & Sandford (1998b).

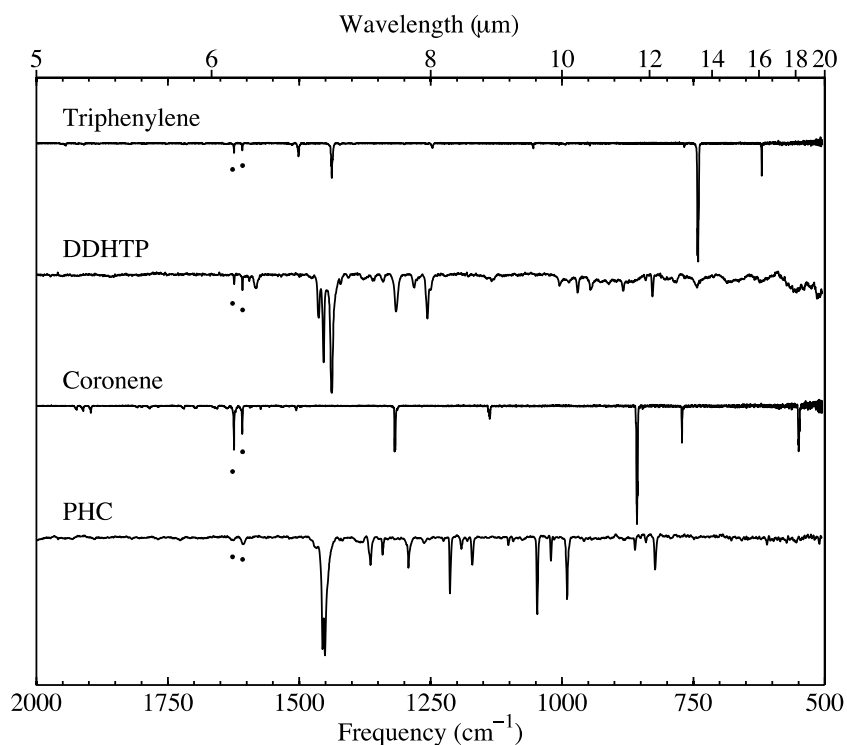


**Figure 18.** The 2000–500  $\text{cm}^{-1}$  spectral region transmission spectra of molecules in Series F. The spectrum of triphenylene is taken from Hudgins & Sandford (1998a) and coronene is taken from Hudgins & Sandford (1998b). A (•) denotes bands due to trace H<sub>2</sub>O contamination.

and scissoring bands from around 1469–1424  $\text{cm}^{-1}$ . Coronene possesses two prominent modes near 550 and 772  $\text{cm}^{-1}$  that are associated with carbon skeletal deformation modes (Hudgins & Sandford 1998b). Coronene has strong, narrow duet C–H<sub>OOP</sub>

bend around 857  $\text{cm}^{-1}$ . There are two prominent bands around 1138 and 1317 that are associated with C–H in-plane bending and aromatic carbon skeletal stretching (Hudgins & Sandford 1998b). Perhydrocoronene possesses complex IR spectrum from

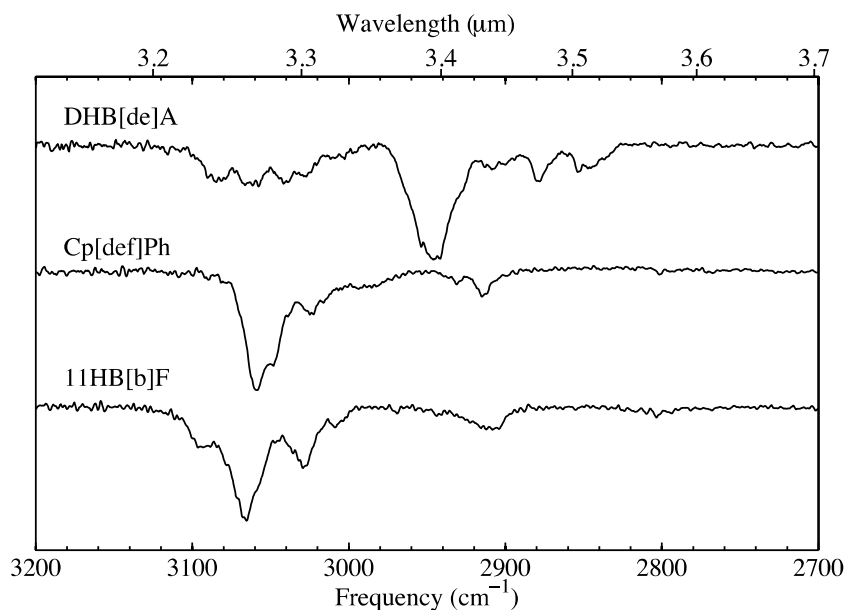


Figure 19. The 3200–2700  $\text{cm}^{-1}$  CH stretch region transmission spectra of molecules in Series G.

Table 20  
5,6-dihydro-4H-benzo[de]anthracene (DHB[de]A)

Band Position ( $\text{cm}^{-1}$ )	Normalized Band Area
518.5	0.05
649.3	0.05
747.7	<b>1.00</b>
758.9	0.60
782.2, 776.0*	0.14
828.2	0.08
843.3	0.15
887.1	0.22
914.3	0.05
944.5, 940.2	0.05
1041.1, 1034.6	0.07
1204.4	0.05
1258.5	0.14
1300.5	0.05
1390.2	0.10
1436.0	0.08
1445.3	0.07
1460.0*, 1453.9	0.36
1498.1	0.14
1592.5(sh), 1590.4*	0.12 <sup>a</sup>
1598.9	0.07 <sup>a</sup>
1630.8	0.11 <sup>a</sup>
(2979–2825): 2945.8*, 2907.9, 2899.8, 2878.7, 2852.8, 2845.0	2.93
(3122–2979): 3083.3, 3061.8, 3041.1, 3027.4	1.46

Note. <sup>a</sup> These strengths are somewhat uncertain due to varying degrees of overlap with bands due to contaminant  $\text{H}_2\text{O}$ .

Table 21  
4H-cyclopenta[def]phenanthrene (Cp[def]Ph)

Band Position ( $\text{cm}^{-1}$ )	Normalized Band Area
699.8	0.23
748.9	0.75
772.1	0.11
823.0(sh), 816.2*	<b>1.00</b>
881.4	0.08
1060.8, 1051.8*	0.10
(1417–1384): 1411.6, 1407.5, 1399.6	0.20
1424.0	0.20
1445.2	0.16
1598.8, 1591.1	0.18 <sup>a</sup>
1772.6, 1767.8	0.05
(1861–1825): 1856.7, 1843.0, 1829.4	0.06
(1935–1893): 1923.9*, 1916.1*, 1905.0	0.12
(2949–2891): 2931.1, 2914.9*	0.20
(3100–2964): 3058.7*, 3048.0, 3023.8, 2984(b)	1.87

Note. <sup>a</sup> An approximate 5% contribution from absorption by contaminant  $\text{H}_2\text{O}$  has been removed.

1490 to  $810 \text{ cm}^{-1}$ . The features between 1463 and  $1434 \text{ cm}^{-1}$  are likely caused by methylene scissoring.

#### A.6. Series G (DHB[de]A, Cp[def]Ph, 11HB[b]F)

The 3200–2700 and 2000–500  $\text{cm}^{-1}$  spectra of matrix isolated DHB[de]A, Cp[def]Ph, and 11HB[b]F are presented in Figures 19 and 20, respectively. The positions and relative strengths of absorption bands associated with the spectra of these molecules are listed in Tables 20–22.

**Table 22**  
11H-benzo[b]fluorene (11HB[b]F)

Band Position ( $\text{cm}^{-1}$ )	Normalized Band Area
570.8	0.17
605.3	0.06
725.4*, 717.1	<b>1.00</b>
742.6	0.28
762.5*, 758.0	0.69
771.5	0.86
817.7*, 812.9	0.05
869.2*, 860.3	0.76
885.8	0.06
955.6*, 948.4	0.24
1023.7*, 1020.1	0.17
1117.7	0.07
1143.7*, 1140.4	0.10
1156.1, 1151.9	0.08
1190.9	0.16
1204.8, 1200.6*	0.06
1226.2	0.05
1266.9	0.14
1315.1	0.21
1342.7	0.08
(1424–1407): 1419.7, 1414.3*, 1408.0(sh)	0.32
(1456–1431): 1452.9, 1446.8, 1442.1*, 1437.6*	0.46
1479.3, 1474.6*	0.27
1506.8*, 1498.9	0.47
1583.0	0.09
(1620–1606): 1616.7, 1612.7, 1608.2	0.06
1813.5	0.06
1899.7	0.05
1945.0, 1940.8	0.09
2907.0	0.23
(3121–2995): 3092.8, 3065.4*, 3027.7, 3008.3	2.95

All three molecules display both aromatic and aliphatic C–H stretch features. DHB[de]A possesses aromatic bands from 3122 to 2979  $\text{cm}^{-1}$  and aliphatic C–H stretch bands from 2979 to 2825  $\text{cm}^{-1}$ , with the most prominent feature being an aliphatic band that appears around 2946  $\text{cm}^{-1}$ . Cp[def]Ph possesses aromatic bands from 3100 to 2964  $\text{cm}^{-1}$  and small aliphatic C–H stretch bands from 2949 to 2891  $\text{cm}^{-1}$ , with the most prominent feature being an aromatic band that appears at 3059  $\text{cm}^{-1}$ . 11HB[b]F possesses aromatic bands from 3121 to 2995  $\text{cm}^{-1}$  and aliphatic C–H stretch bands from 2979 to 2945  $\text{cm}^{-1}$ , with the most prominent feature being an aromatic band that appears at 3065  $\text{cm}^{-1}$ .

The 900–700  $\text{cm}^{-1}$  region of the spectrum of DHB[de]A is complex with bands at 887.1, 843.3, 828.2, 782.2, 776.0, 758.9, and 747.7  $\text{cm}^{-1}$ . Some of these bands are produced by a lone

**Table 23**  
7,14-dihydrodibenz[ah]anthracene (DHDB[ah]A)

Band Position ( $\text{cm}^{-1}$ )	Normalized Band Area
527.8	0.11
646.5	0.10
677.0, 674.9*	0.25
740.9(sh), 736.5*	0.48
778.2	0.08
815.3, 809.1*	<b>1.00</b>
(1043–1029): 1040.8, 1036.7, 1032.9	0.08
1145.4, 1137.9	0.07
1185.9, 1181.3, 1178.7*	0.20
1407.3*, 1401.9	0.34
1483.2	0.08
1515.2	0.28
1582.4	0.05
1608.0	0.19 <sup>a</sup>
1631.5	0.14
2827.9	0.17
2883.7	0.28
(3146–2990): 3097.0, 3075.3*, 3065.2*, 3046.8	2.00

**Note.** <sup>a</sup> An approximate 5% contribution from absorption by contaminant  $\text{H}_2\text{O}$  has been removed.

quartet, a lone trio, and solo C–H<sub>OOP</sub> bending mode vibrations. Cp[def]Ph has triplet C–H<sub>OOP</sub> bands at 772.1 and 748.9  $\text{cm}^{-1}$  and a duet band at 823.0 and 816.2  $\text{cm}^{-1}$ . 11HB[b]F has at least five bands within the quartet C–H<sub>OOP</sub> bending region at 771.5, 762.5, 758.0, 742.6, and 725.4  $\text{cm}^{-1}$ , in addition to solo bands at 869.2 and 860.3  $\text{cm}^{-1}$ . For all three molecules, the region between 1600 and 1000  $\text{cm}^{-1}$  is a combination of C–H in-plane bending, aromatic carbon skeletal stretching, methylene scissoring modes, and overtones/combinations of lower frequency modes.

#### A.7. Series H (DHDB[ah]A, B[e]P, DHB[e]P, TRIP):

The 3200–2700 and 2000–500  $\text{cm}^{-1}$  spectra of matrix isolated DHDB[ah]A, B[e]P, DHB[e]P, and TRIP are presented in Figures 21 and 22, respectively. The positions and relative strengths of absorption bands associated with the spectra of these molecules are listed in Tables 23–25.

The spectrum of DHDB[ah]A shows two aliphatic C–H stretch bands centered around 2883.7 and 2827.9  $\text{cm}^{-1}$  with a broad aromatic C–H stretch feature from 3146 to 2990  $\text{cm}^{-1}$ . The spectrum of B[e]P possesses only aromatic C–H stretch bands from 3130 to 3010  $\text{cm}^{-1}$ , with the largest band centered near 3061.3  $\text{cm}^{-1}$  (Hudgins & Sandford 1998b). The profile of the aromatic features of DHB[e]P is similar to that found in B[e]P, although the feature only spans 3118–2999  $\text{cm}^{-1}$ . The aliphatic bands in DHB[e]P are broad, spanning the region from 2999 to 2808  $\text{cm}^{-1}$ . The spectrum of TRIP has a complex aromatic C–H stretch region with bands ranging from 3114 to 3000  $\text{cm}^{-1}$ . The aliphatic C–H stretch in TRIP is

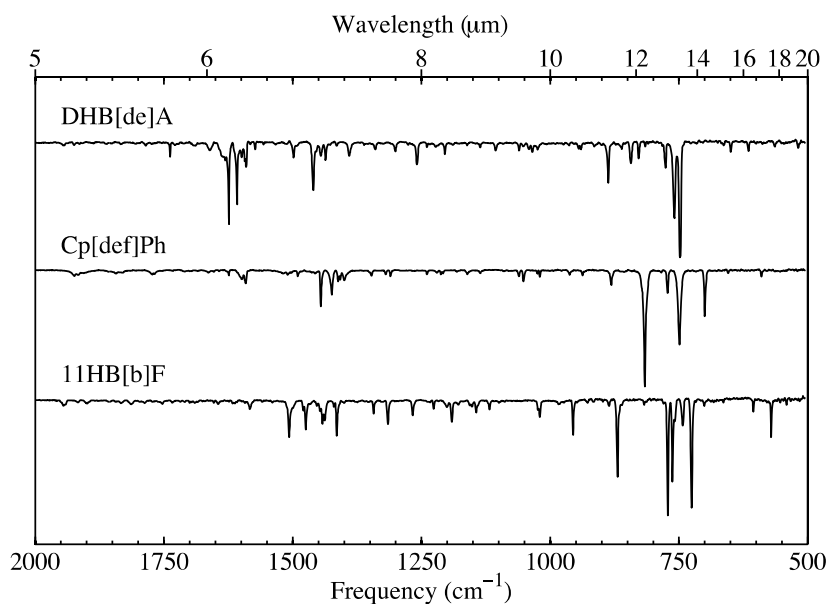


**Figure 20.** The 2000–500  $\text{cm}^{-1}$  spectral region transmission spectra of molecules in Series G.

**Table 24**  
9,10-dihydrobenzo[e]pyrene (DHB[e]P)

Band Position ( $\text{cm}^{-1}$ )	Normalized Band Area
526.2	0.07
559.1, 554.2	0.07
593.9	0.08
605.3	0.05
635.2	0.06
674.9	0.34
690.6	0.06
715.2	0.32
722.6	0.54
756.1	0.40
778.4	0.09
828.6	<b>1.00</b>
895.5	0.07
915.0, 911.2	0.09
939.8	0.05
1002.4	0.06
1024.2	0.05
1070.6, 1065.6	0.05
(1116–1097): 1109.6*, 1103.6, 1100.5	0.21
1191.3*, 1188(sh)	0.18
1243.1*, 1237.7	0.09
1402.2	0.08
1428.8*, 1425(sh)	0.10
1442.9, 1439.4	0.16
1469.9	0.16
1591.0	0.13 <sup>a</sup>
1601.8	0.09
1767.3*, 1764.9	0.08

**Table 24**  
(Continued)

Band Position ( $\text{cm}^{-1}$ )	Normalized Band Area
1782.8	0.09
1927.6	0.05
(2999–2808): 2969(sh), 2953.1*, 2941.0, 2889.8, 2840.5	2.41
(3118–2999): 3095.4, 3079.5, 3057.3*, 3046.9, 3026.7	1.62

**Note.** <sup>a</sup> An approximate 40% contribution from absorption by contaminant  $\text{H}_2\text{O}$  has been removed.

**Table 25**  
Triptycene (TRIP)

Band Position ( $\text{cm}^{-1}$ )	Normalized Band Area
626.2*, 623.8	0.57
742.4	<b>1.00</b>
796.7*, 792(sh)	0.15
(1175–1156): 1171.5, 1169.0 1166.2*, 1162.4, 1159.1	0.11
(1206–1186): 1201.5, 1197.3*, 1193.2*	0.19
(1475–1448): 1469.0, 1460.4*, 1454(sh)	0.66
(2998–2946): 2991.1, 2958.3*	0.20 <sup>a</sup>
(3114–3000): 3081.5*, 3076(sh), 3070.0, 3058.7, 3049.4, 3028.6*, 3014.9	0.84

**Note.** <sup>a</sup> The 2958.3  $\text{cm}^{-1}$  band has an unusual, large, high frequency wing.

relatively simple with the primary feature spanning the region of 2998–2946  $\text{cm}^{-1}$  with a peak at 2958.3  $\text{cm}^{-1}$ .

At longer wavelengths, there are three bands in the C–H<sub>oop</sub> bending region of the spectrum of DHDB[ah]A, which

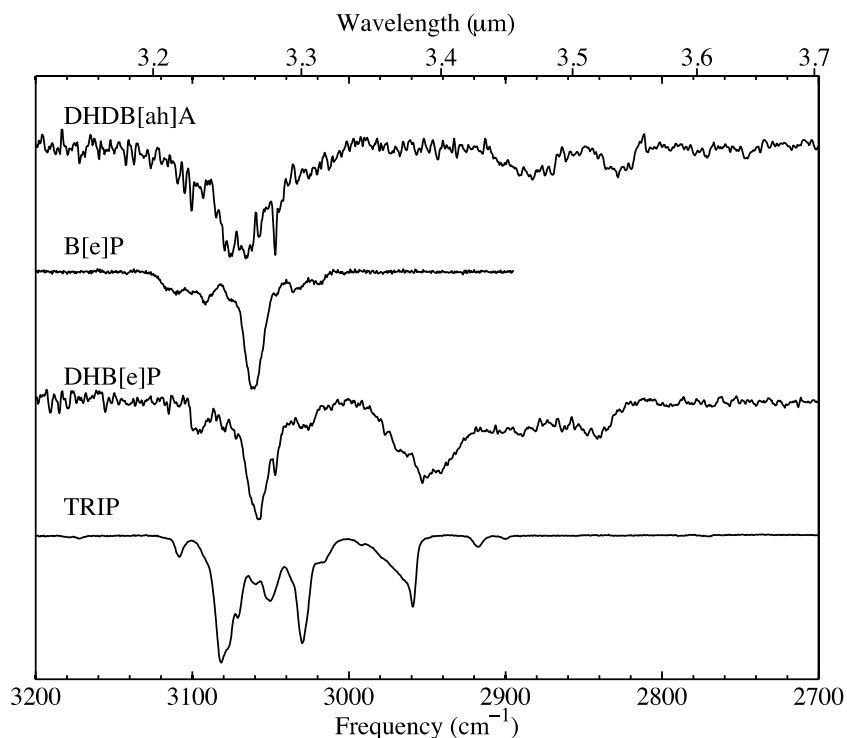


**Figure 21.** The 3200–2700 cm<sup>-1</sup> CH stretch region transmission spectra of molecules in Series H. The spectrum of benzo(e)pyrene is taken from Hudgins & Sandford (1998b).

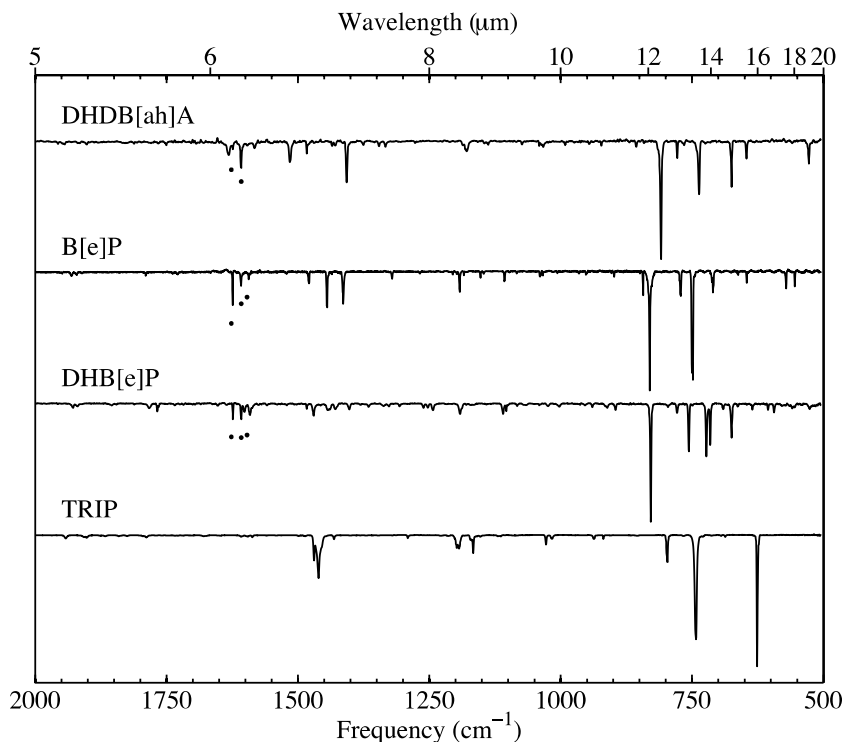


**Figure 22.** The 2000–500 cm<sup>-1</sup> spectral region transmission spectra of molecules in Series H. The spectrum of benzo(e)pyrene is taken from Hudgins & Sandford (1998b). A (\*) denotes bands due to trace H<sub>2</sub>O contamination.

possesses quartet and duet aromatic hydrogens, at 815.3, 809.1, 778.2, 740.9, and 736.5 cm<sup>-1</sup>. The C–H<sub>OOP</sub> bending region of B[e]P has bands at 843.0, 830.4, 771.8, 750.0, and 710.5 cm<sup>-1</sup> some of which can be attributed to quartet, trio, and duet aromatic hydrogens (Hudgins & Sandford 1998b). In DHB[e]P, the

quartet band is lost leaving only trio, duet, and olefinic C–H<sub>OOP</sub> modes. The main bands in this region of the DHB[e]P spectrum lie at 828.6, 778.4, 756.1, 722.6, and 715.2 cm<sup>-1</sup>. In TRIP the only C–H<sub>OOP</sub> band, which is associated with quartet hydrogens, is found at 742.4 cm<sup>-1</sup>.

## REFERENCES

- Aléon, J., Engrand, C., Robert, F., & Chaussidon, M. 2000, *M&PS*, **35**, A19
- Allamandola, L. J., Bregman, J. D., Sandford, S. A., et al. 1989a, *ApJL*, **345**, L59
- Allamandola, L. J., Hudgins, D. M., & Sandford, S. A. 1999, *ApJL*, **511**, L115
- Allamandola, L. J., Tielens, A. G. G. M., & Barker, J. R. 1985, *ApJL*, **290**, L25
- Allamandola, L. J., Tielens, A. G. G. M., & Barker, J. R. 1989b, *ApJS*, **71**, 733
- Arnoult, K. M., Wdowiak, T. J., & Beegle, L. W. 2000, *ApJ*, **535**, 815
- Barker, J. R., Allamandola, L. J., & Tielens, A. G. G. M. 1987, *ApJL*, **315**, L61
- Bauschlicher, C. W., Jr., Langhoff, S. R., Sandford, S. A., & Hudgins, D. M. 1997, *JPhCh*, **101**, 2414
- Bernstein, M. P., Elsila, J. E., Dworkin, J. P., et al. 2002, *ApJ*, **576**, 1115
- Bernstein, M. P., Sandford, S. A., & Allamandola, L. J. 1996, *ApJL*, **472**, L127
- Bernstein, M. P., Sandford, S. A., Allamandola, L. J., et al. 1999, *Sci*, **283**, 1135
- Bernstein, M. P., Sandford, S. A., & Allamandola, L. J. 2005, *ApJS*, **161**, 53
- Clemett, S., Maechling, C., Zare, R., Swan, P., & Walker, R. 1993, *Sci*, **262**, 721
- Colthup, N. B., Daly, L. H., & Wiberley, S. E. 1990, *Introduction to Infrared and Raman Spectroscopy* (San Diego, CA: Academic), 228
- Cronin, J. R., Pizzarello, S., Epstein, S., & Krishnamurthy, R. V. 1993, *GeCoA*, **57**, 4745
- Epstein, S., Krishnamurthy, R. V., Cronin, J. R., Pizzarello, S., & Yuen, G. U. 1987, *Natur*, **326**, 477
- Geballe, T. R., Tielens, A. G. G. M., Kwok, S., & Hrivnak, B. J. 1992, *ApJL*, **387**, L89
- Halasinski, T. M., Salama, F., & Allamandola, L. J. 2005, *ApJ*, **628**, 555
- Hudgins, D. M., & Allamandola, L. J. 1995a, *JPhCh*, **99**, 3033
- Hudgins, D. M., & Allamandola, L. J. 1995b, *JPhCh*, **99**, 8978
- Hudgins, D. M., & Allamandola, L. J. 1997, *JPhCh*, **101**, 3472
- Hudgins, D. M., & Sandford, S. A. 1998a, *JPhCh*, **102**, 329
- Hudgins, D. M., & Sandford, S. A. 1998b, *JPhCh*, **102**, 344
- Hudgins, D. M., & Sandford, S. A. 1998c, *JPhCh*, **102**, 353
- Hudgins, D. M., Sandford, S. A., & Allamandola, L. J. 1994, *JPhCh*, **98**, 4243
- Jourdain de Muizon, M., Geballe, T. R., d'Hendecourt, L. B., & Baas, F. 1986, *ApJL*, **306**, L105
- Jourdain de Muizon, M., d'Hendecourt, L. B., & Geballe, T. R. 1990, *A&A*, **235**, 367
- Kerridge, J. F., Chang, S., & Shipp, R. 1987, *GeCoA*, **51**, 2527
- Langhoff, S. R., Bauschlicher, C. W., Jr., Hudgins, D. M., Sandford, S. A., & Allamandola, L. J. 1998, *JPhCh*, **102**, 1632
- Mattioda, A. L., Hudgins, D. M., Bauschlicher, C. W., Rosi, M., & Allamandola, L. J. 2003, *JPhCh*, **107**, 1486
- McKeegan, K. D., Aléon, J., Bradley, J., et al. 2006, *Sci*, **314**, 1724
- McKeegan, K. D., Walker, R. M., & Zinner, E. 1985, *GeCoA*, **49**, 1971
- Messenger, S. 2000, *Natur*, **404**, 968
- Peeters, E., Allamandola, L. J., Bauschlicher, C. W., Jr., et al. 2004, *ApJ*, **604**, 252
- Peeters, E., Hony, S., van Kerckhoven, C., et al. 2002, *A&A*, **390**, 1089
- Quinkert, G., Egert, E., & Griesinger, C. 1996, *Aspects of Organic Chemistry: Structure* (New York, NY: Wiley-VCH), 102
- Sandford, S. A. 1991, *ApJ*, **376**, 599
- Sandford, S. A. 2002, *P&SS*, **50**, 1145
- Sandford, S. A., Allamandola, L. J., Tielens, A. G. G. M., et al. 1991, *ApJ*, **371**, 607
- Sandford, S. A., Bernstein, M. P., Allamandola, L. J., Gillette, J. S., & Zare, R. N. 2000, *ApJ*, **538**, 691
- Sandford, S. A., Bernstein, M. P., & Dworkin, J. P. 2001, *M&PS*, **36**, 1117
- Silverstein, R. M., & Bassler, G. C. 1967, *Spectrometric Identification of Organic Compounds* (2nd ed.; New York: Wiley)
- Sloan, G. C., Bregman, J. D., Geballe, T. R., Allamandola, L. J., & Woodward, C. E. 1997, *ApJ*, **474**, 735
- Szczepanski, J., Banisaukas, J., Vala, M., et al. 2002, *JPhCh*, **106**, 63
- Tielens, A. G. G. M. 2008, *ARA&A*, **46**, 289
- Wagner, D. R., Kim, H. S., & Saykally, R. J. 2000, *ApJ*, **545**, 854
- Wexler, A. S. 1967, *ApSRv*, **1**, 29
- Witteborn, F. C., Sandford, S. A., Bregman, J. D., et al. 1989, *ApJ*, **341**, 270
- Zinner, E. 1988, in *Meteorites and the Early Solar System*, ed. J. F. Kerridge & M. S. Matthews (Tucson, AZ: Univ. Arizona Press), 956